Control of T-Type Multilevel Inverter Fed PMSM Drives Using Hybrid ANFIS-FCS-MPCC Technique for EV Application

Anchal Raghuwanshi[1]*, Amit Ojha[2],

[1*, 2] Department of Electrical Engineering, Maulana Azad National Institute of Technology, Bhopal-462003, India.

*Corresponding author: 213113001@stu.manit.ac.in[1], +918085239665;

Contributing author: Amitojha@manit.ac.in[2].

Abstract—This paper presents an advanced hybrid control approach combining Adaptive Neuro-Fuzzy Inference System (ANFIS) and Finite Control Set Model Predictive Current Control (FCS-MPCC) for a T-type multilevel inverter (T-MLI)-driven Permanent Magnet Synchronous Motor (PMSM) for Electric Vehicle (EV) application. The proposed Hybrid ANFIS-FCS-MPCC technique, alongside the T-MLI, is designed to enhance the power quality and improve the motor response by reducing the torque ripples, noise-vibration harshness (NVH), and improving the transient and steady-state response. The proposed technique resulted in a notable reduction, including a 66% drop in torque oscillations, a 50% reduction in speed overshoots, and a 33% minimization of current harmonic distortion, in comparison to the conventional MPCC methodology. MATLAB/SIMULINK platform is used to simulate the proposed technique and a prototype is developed in the laboratory to validate the efficacy of the proposed technique, Further, a comparative analysis is performed with the conventional techniques to show the effectiveness of the proposed technique in terms of motor speed, torque ripples, and stator current response.

Index Terms— Adaptive Neuro-Fuzzy Inference System (ANFIS), Electric vehicle (EV), Model predictive current control (MPCC), Permanent magnet synchronous motor (PMSM), T-type multilevel inverter (T-MLI).

1. INTRODUCTION

Recently, the EV drive system has primarily relied on the conventional two-level inverter (2L-I) structure. The devices within a 2L-I generate high dv/dt stress and introduce harmonics into the inverter's voltage output. To address this issue, a bulky LC filter is typically required. [1]. However, for EV applications, it is crucial that the filter size is kept to a minimum. Alternatively, maintaining a high switching frequency (SF) can help reduce the need for filters. Nevertheless, higher switching frequencies also lead to increased switching losses, which present a significant challenge in the automobile industry [2]. Additionally, higher voltage semiconductor devices are necessary for 2L-I systems with elevated DC link voltages, which further increases conduction losses and, consequently, reduces overall efficiency.

Multi-level inverters (MLIs) exhibit lower harmonic content and diminished voltage stress in comparison to two-level inverters (2L-I). A review of the literature has been conducted to identify suitable MLI topologies [1], [3], [4], [5], [6]. The main MLI topologies consist of neutral point diode clamped (NPC), T-type, flying capacitor (FC), and cascaded H-bridge (CHB) inverters. [7]. Some literature indicates that CHB MLI is employed for EV applications; however, the necessity for isolated DC sources for each phase limits its use in this context. In contrast, FC is frequently employed for filtration and enhancing power factor; however, the significant size of the capacitor makes it more expensive and unwieldy [8]. A 5-level NPC inverter is employed for the PMSM drive in [9], incorporating clamped diodes, which results in a higher device count and diminished system reliability. Compared to T-MLI, the NPC inverter has two extra diodes for generating three levels, which is a limitation of NPC. The 3LIs adequately balance the Total Harmonic Distortion (THD), cost, reliability, and system size for EV applications. The T-MLI serves as a viable alternative among various multilevel inverter topologies [10]. CHB, FC, and NPC are unsuitable for EV applications because of the abovementioned issues.

The 3-phase 3-level voltage source inverters (VSIs) have gained increased popularity and application compared to the 2-level inverters. This is due to their ability to provide higher-quality electrical energy and reduce the dv/dt stress on power devices. The T-MLI represents the optimal alternative to 2L-I due to its superior efficiency and reduced conduction losses. The fundamental T-MLI was presented in [11] for low and medium-voltage applications. This inverter features an active bidirectional switch positioned between the DC link's midpoint and the phase leg of the conventional 2L-I topology, aimed at improving output voltage quality. In comparison to the 3L-NPC inverter, this design removes the necessity for clamping diodes, thereby decreasing the total number

of components and the requirements for reactive power. This leads to enhanced power quality and increased efficiency at the output of the inverter. Figure 1 depicts the three-level T-MLI (3L-TI).

PMSM and Induction Motors (IM) are extensively utilized in electric EVs to meet traction requirements. But nowadays, PMSM has replaced the IM because it has permanent magnets (PMs) with high power density, which reduces the weight as well as the size of the motor. Besides this, PMSMs are widely used for their higher torque density, higher ratio of torque to inertia, and high-speed operating capabilities [12], [13].

Various types of control strategies for PMSM are reviewed [14], [15], [16], [17], [18]. Fuzzy logic controllers have been most adopted among all types of controllers with high accuracy, reliability, and adaptability [19]. Artificial intelligence techniques are used nowadays to design highly efficient and adaptive controllers. The ANFIS technique [20] combines fuzzy and neural network features to control the system variables and generate a rapid and stable control action. ANFIS has been utilized in previous literature for different kinds of applications. [21] has controlled the EV by ANFIS considering the battery State of charge, [22] proposed a speed control method using a recurrent neural network for PMSM drives. The ANFIS is an intelligent control strategy that includes the benefits of both neural networks and fuzzy logic. The ANFIS as an outer speed controller in PMSM drives can effectively handle the nonlinearities due to factors like magnetic saturation, load variations, and changes in motor parameters with temperature. ANFIS has adaptive learning capabilities for changing conditions in the motor and drive system, and it continuously tunes its parameters to enhance the system's performance. The fuzzy inference system within ANFIS allows for a more nuanced decision-making process than binary logic, which is especially useful in dealing with the inherent uncertainties and variabilities in motor operation.

Model Predictive Control (MPC) has garnered significant focus due to its advanced capabilities, like multivariable control utilizing a single loop, and quick dynamic response with consideration of nonlinearities and their restrictions, and it is considered to be one of the most desirable control schemes for PMSMs [23], [24] in a variety of industrial applications, like traction, electric ship propulsion, wind power generators, and more. The MPC is a more effective method than direct torque control (DTC) and traditional field-oriented control (FOC) because of its ability to handle multi-objective optimization problems.

Various types of MPC techniques have been presented in [25], [26]. The MPC is categorized into Direct and Indirect MPC. In the Direct MPC, the controller outputs are the switching vectors, which act as an integer vector and are directly provided to the inverter without the requirement of a modulator. However, Indirect MPC produces output as a vector of real values, and the switching pulses are produced by a modulator after the control action.

These MPC approaches may be further divided into two categories. FCS-MPC is a direct MPC method, while Continuous control set (CCS) MPC is an indirect one [27]. The CCS-MPC requires a modulator to generate the gate pulses. CCS-MPC's advantage is that it can deliver a fixed SF. However, the design of the optimization issue is complex, especially for bilinear systems such as MLI topologies. Unlike CCS-MPC, the FCS-MPC approach can obtain an optimal switching vector without the requirement for a modulator. It has a basic design and excellent dynamic performance. The FCS-MPC approach properly follows the required current or torque/flux by considering all available switching vectors. This technique is obvious and simple to use in the design and execution processes.

However, because the FCS-MPC lacks a modulator, the optimization process immediately selects the switching vector to monitor the reference of control variables. This results in an unpredictable SF of semiconductor switches [28]. This problem is a frequent limitation of FCS-MPC techniques. If no constraints are considered to regulate the SF, the resulting output current will exhibit a random-like spectrum and be dispersed throughout a large range.

Due to the absence of defined frequencies for allocating the harmonics of the output voltage, designing the filters for the converter's output will be challenging. Furthermore, the heat sink design must be proper, failing in it, might be detrimental to PMSM drives in applications where there is compact space, such as in EV applications. Keeping in mind, the above-mentioned problems, the FCS-MPCC is implemented as an inner current control loop, which also diminishes the requirement of a modulator and provides a minimum switching transition optimal switching vector as the output, which triggers the semiconductor devices of the 3L-T-type inverter.

The originality of the proposed control technique and the contributions of the author are summarized as follows:

a) Development of a novel speed and current control strategy for PMSM drives, utilizing an ANFIS-FCS-MPCC hybrid approach. This advanced controller controls the speed error as well as the rate of change of speed error, demonstrating enhanced performance in control precision and trajectory tracking across various operating scenarios.

b) Implementation of a Three-level T-type inverter with the proposed technique replacing the two-level VSI to reduce the harmonic distortions at the output side of the inverter and improve the overall quality of power delivered to the PMSM.

c) Assessment of the dynamic performance of the laboratory PMSM drive prototype under variable operating circumstances, using the proposed ANFIS-FCS-MPCC in contrast to other control methodologies. The proposed technique resulted in a notable reduction, including a 66% drop in torque oscillations, a 50% reduction in speed overshoots, and a 33% minimization of current harmonic distortion, in comparison to the conventional MPCC methodology.

2. T-TYPE MULTILEVEL INVERTER DRIVEN-PMSM DRIVES USING HYBRID ANFIS-FCS-MPCC TECHNIQUE

2.1 3L-T-Type Inverter

The 3L-TI-fed PMSM drive system is presented in Figure1. All three individual phases of the inverter have four IGBTs $S_{1x} - S_{4x}$ $(x = a, b, c)$, where (S_{1x}, S_{4x}) and (S_{2x}, S_{3x}) are complementary switches. There are three operational states for the 3L-TI: positive [1], zero [0], and negative [-1], as depicted in Table 1.

S_m is the switching vector matrix of phases a, b, and c given by

$$S_m = \begin{bmatrix} S_a & S_b & S_c \end{bmatrix}^T \tag{1}$$

The space vector diagram of 3L-TI with 27 switching states is presented in Figure2. Assuming that the voltage of capacitors V_{c1} and V_{c2} is same, the output V_{xn} w.r.t. the neutral N will be $V_{dc}/2$, 0, and $-V_{dc}/2$ respectively.

2.2 Modelling of PMSM

The mathematical modeling of PMSM in a synchronously rotating frame (dq-axis reference frame) can be written as

$$u_d = i_d R_s + L_d \frac{di_d}{dt} - \omega_e (i_q L_q) \tag{2}$$

$$u_q = i_q R_s + L_q \frac{di_q}{dt} + \omega_e \left(\lambda_{PM} + i_d L_d\right) \tag{3}$$

$$T_e = \frac{3}{2} p i_q \left[\left(L_d - L_q\right) i_d + \lambda_{PM}\right] \tag{4}$$

Since the surface-mounted PMSM has equal values of L_d and L_q Therefore, the equation. (2), (3), and (4) respectively can be modified as

$$\frac{di_d}{dt} = -\left(\frac{R_s}{L_d}\right) i_d + \left(\frac{1}{L_d}\right) u_d + \left(\frac{L_q}{L_d}\right) \omega_e i_q \tag{5}$$

$$\frac{di_q}{dt} = -\left(\frac{R_s}{L_q}\right) i_q + \left(\frac{1}{L_q}\right) u_q - \left(\frac{L_d}{L_q}\right) \omega_e i_d - \frac{\omega_e \lambda_{PM}}{L_d} \tag{6}$$

$$T_e = \frac{3}{2} p i_q \lambda_{PM} \tag{7}$$

Where the voltages of the d-axis and q-axis are denoted by u_d & u_q respectively; L_d & L_q are stator inductance; Stator resistance is denoted by R_s ; i_d & i_q are dq-axis stator currents; T_e is the electromagnetic torque (Nm) of PMSM; ω_e is the electrical angular speed (rad/sec) of PMSM; p is the number of pairs of poles of PMs on the rotor and λ_{PM} is the flux linkage of PMs (Wb).

2.3 PI Controller Laws:

Outer Loop Speed Control:

$$i_q^* = K_{p\omega} e_\omega + K_{i\omega} \int e_\omega dt \tag{8}$$

Inner Loop Current Control:

$$v_d^* = K_{pd} e_{id} + K_{id} \int e_{id} dt \tag{9}$$

$$v_q^* = K_{pq} e_{iq} + K_{iq} \int e_{iq} dt \tag{10}$$

The PI controller gains are calculated using the Ziegler-Nichols (ZN) method in Section V. e_ω be the speed error, i.e., the difference between the reference and actual speed. e_{id} and e_{iq} are the errors in the d & q axes components of the stator current of the PMSM. These outputs v_d^* and v_q^* are fed to the PWM generator. The main limitations of the PI controller-based vector control method are that it assumes the system is linear, requires accurate parameters, and is not adaptive to disturbances and nonlinearities.

3. ANFIS CONTROLLER

ANFIS was first introduced in [20]. It incorporates the human-like analytical approach of fuzzy systems with neural networks' learning and adaptability features. The system is based on a fuzzy inference system (FIS) and utilizes a hybrid learning approach that optimizes the membership function (MF) parameters using both gradient descent and least-squares estimation. The structure of the ANFIS controller is presented in Figure 3.

ANFIS as an Outer Speed Controller: In a PMSM drive, the control strategy is often divided into two loops, i.e., inner, and outer control loops. The inner Current Control Loop manages the motor's current and ensures that it follows the reference current signals. It typically uses a Proportional-Integral (PI) controller, which MPCC replaces in the proposed system because of the aforementioned advantages of MPCC. The speed control loop also uses a PI controller, which generates the reference i_q current signal is based on the speed error, but it is not adaptive and robust, due to which there are very high ripples in the reference i_q, which complicates the operation of the inner control loop. To mitigate these limitations, the proposed control system implemented the ANFIS control as the outer speed controller. It takes input of speed error as well as the rate of change of speed error. The architecture of an ANFIS is typically as a speed controller presented in Figure 4.

It includes the Takagi-Sugeno inference system to generate the following if-then rules:

$x = \mu_A^1$ & $y = \mu_B^1$, $i = 1$, (Rule 1)

$$f_1 = (p_1.x) + (q_1.y) + r_1 \tag{11}$$

$x = \mu_A^2$ & $y = \mu_B^2$, $i = 2$, (Rule 2)

$$f_2 = (p_2.x) + (q_2.y) + r_2 \tag{12}$$

Where: p_i, q_i, & r_i be the consequent parameters to be optimized through training, and $\mu_A^1, \mu_A^2, \mu_B^1, \mu_B^2$ are the MFs.

a) **Fuzzification or Input Layer: (Layer 1)** - In this layer, the speed error (e_ω) and its rate of change ($\dot{e}_\omega$) are taken as inputs. This layer is also known as the Fuzzification layer. MFs are used on these inputs to produce fuzzy values. Each neuron represents an MF in this layer. If the inputs to the layer are $x = e_\omega$, (error in speed) and $y = \dot{e}_\omega$, (rate of change in speed error), then

$$O_{1A}^i = \mu_A^i(e_\omega) \tag{13}$$

$$O_{1B}^{i} = \mu_{B}^{i}(\dot{\omega}) \tag{14}$$

Where: O_{1A}^{i} and O_{1B}^{i} are the outputs of neurons in layer 1, $\mu_{A}^{i}(e_{\omega})$ is the MF for the speed error, $\mu_{B}^{i}(\dot{\omega})$ is the MF for the rate of change in the speed error.

b) Rule Layer (Product of Membership Degrees): (Layer 2) - At this layer, each node computes the firing strength (or weight) of a fuzzy rule using the "AND" operator, which is generally the product of the membership degrees from layer 1. The layer 2's output of the i[th] rule neuron is:

$$O_{2}^{i} = W_{i} = \mu_{A}^{i}(e_{\omega}) * \mu_{B}^{i}(\dot{\omega}) \tag{15}$$

Where: W_i is the weight of the i[th] rule, $\mu_{A}^{i}(e_{\omega})$ and $\mu_{B}^{i}(\dot{\omega})$ are the layer 1 MFs.

c) Normalization: (Layer 3) - In this layer, the firing strengths are normalized. Each neuron computes the ratio of the i[th] rule's weight to the sum of all weights.

$$O_{3}^{i} = \overline{W}_{i} = \frac{W_{i}}{\sum_{i} W_{i}} \tag{16}$$

$$O_{3}^{i} = \overline{W}_{i} = \frac{W_{i}}{W_{1} + W_{2}} \tag{17}$$

Where, $\overline{W}_{i}$ is the normalized weight of the i[th] rule.

d) Defuzzification Layer: (Layer 4) - Each neuron calculates the i[th] fuzzy rule output. The output is the multiple of the normalized weight and a 1[st] order linear function of the inputs e_{ω} and $\dot{\omega}$.

$$f_{i} = p_{i} e_{\omega} + q_{i} \dot{\omega} + r_{i} \tag{18}$$

$$O_{4}^{i} = \left(\overline{W}_{i} f_{i}\right) = \overline{W}_{i} (p_{i} e_{\omega} + q_{i} \dot{\omega} + r_{i}) \tag{19}$$

e) Output Layer: (Layer 5) - This layer adds up the outputs from all neurons in Layer 4 to produce the final output of the controller, which acts as the reference i_q current signal for the PMSM drive.

$$i_{q}^{*} = O_{5} \tag{20}$$

The output of this layer is the reference signal for the PMSM drive's inner current control loop.

Using trained data, ANFIS training is carried out offline using the ANFIS editor in MATLAB software. The gradient descent approach and least square estimation (LSE) are used in the simulation. The workspace containing the input-output data pattern is where the ANFIS training dataset is found. Using this data, experiments are performed to check the proposed ANFIS-FCS-MPCC technique for the 3L-TI-fed PMSM drive's performance under different operating situations.

4. FCS-MPCC TECHNIQUE

4.1 PMSM Current Prediction Model

The classic PMSM current prediction model is represented by converting its continuous mathematical model from Equations (5) and (6), assuming the T_s be the sample time of the system and implementing the Forward Euler discretization method yield the predicted values of the current.

$$i_{d}(k+1) = \left(\frac{T_{s}}{L_{d}}\right) u_{d}(k) + \left(1 - \frac{R_{s} T_{s}}{L_{d}}\right) i_{d}(k) + \frac{\omega_{e} L_{q} T_{s}}{L_{d}} i_{q}(k) \tag{21}$$

$$i_q(k+1)=\left(\frac{T_s}{L_q}\right)u_q(k)+\left(1-\frac{R_sT_s}{L_q}\right)i_q(k)-\left(\frac{\omega_e L_d T_s}{L_q}\right)i_d(k)-\left(\frac{\omega_e \lambda_{PM} T_s}{L_q}\right) \quad (22)$$

The computation delay produced by digital signal processors ought to be considered in actual implementation, particularly for multilevel inverters. [29]. Therefore, the current prediction incorporates a compensation of one step to enhance the performance. The currents predicted for $(k+2)^{th}$ Instance can be calculated from $i_d(k+1)$ and $i_q(k+1)$ as

$$i_d(k+2)=\left(\frac{T_s}{L_d}\right)u_d(k+1)+\left(1-\frac{R_sT_s}{L_d}\right)i_d(k+1)+\left(\frac{\omega_e L_q T_s}{L_d}\right)i_q(k) \quad (23)$$

$$i_q(k+2)=\left(\frac{T_s}{L_q}\right)u_q(k+1)+\left(1-\frac{R_sT_s}{L_q}\right)i_q(k+1)-\left(\frac{\omega_e L_d T_s}{L_q}\right)i_d(k)-\left(\frac{\omega_e \lambda_{PM} T_s}{L_q}\right) \quad (24)$$

Thus, depending on the voltage vectors, the applied voltages in the following controlling period will be $u_d(k+1)$ and $u_q(k+1)$. The cost function (C_i) for current control is given as

$$C_i=\left(i_d^*-i_d(k+2)\right)^2+\left(i_q^*-i_q(k+2)\right)^2 \quad (25)$$

This was the basic conventional MPCC technique. It has limitations, like variable and very high switching frequencies. It requires an accurate model of the system without parameter variations [30], [31], [32]. Because of the limited prediction horizon, it provides large steady-state errors. To keep the constant SF, the MPCC method is implemented using a switching penalization technique that keeps track of the minimum switching transitions.

4.2 Penalization on Switching

The practical SF for drives with FCS-MPC depends upon load torque, utilization of the DC-link voltage, sampling frequency, & speed of the motor. Theoretically, the maximum SF of FCS-MPC is around 50% of the sampling frequency. But empirically, it is advised to maintain the sampling frequency of at least 20 times the SF. As a result, the traditional FCS-MPC is advised to penalize switching transitions to reduce the average value of the SF. It can be executed by minimizing the switching vector transitions between the present and next sampling instants as

$$\Delta S_m=\left\|S_m(k-1)-S_m(k)\right\|_1 \quad (26)$$

$$C_{sw}=\Delta S_m \quad (27)$$

where, (C_{sw}) is the cost function for switching vector transition. Due to this switching vector transition penalization technique, the system will be more likely to hold onto its most recent switching vectors during the next control period.

4.3 Overall Cost Function

For the proposed 3L-TI-fed PMSM drive, the overall cost function (C) is:

$$C=C_i+\lambda_{sw}C_{sw} \quad (28)$$

Where λ_{sw} is the weighting factor for switching vector penalization. It is optimized by simulations, and the incremental change was taken as 0.01, the average switching frequency of 5 kHz was recorded at 0.46. Hence, the value of λ_{sw} is taken as 0.46.

Figure 5 presents the complete control diagram for the proposed ANFIS-FCS-MPCC technique. The proposed method replaces the PI controllers in both the inner and outer control loops. Additionally, an optimal switching vector selection method was applied in MPCC to maintain a low average SF, while leveraging the robustness, adaptiveness, and accuracy of ANFIS combined with MPC.

To achieve rolling optimization, all 27 possible switching vectors of the inverter will be assessed, and the best switching vector will be used in the subsequent sampling moment. Given that S_{x1} and S_{x2} are not a pair of complementary switches and could

conduct at the same time in the absence of sufficient dead-band time, it is imperative to tightly forbid state transitions between [1] and [-1] to escape short circuits. Finally, the entire optimization problem can be written as:

$$S_{m_{opt}}(k+1) = \arg\min(C) \tag{29}$$

Such that $S_m \in \{1, 0, -1\}, \Delta S_m \leq 1.$

4.4 Execution

The execution of the proposed ANFIS-FCS-MPCC technique flowchart is presented in Figure 6.

5. RESULTS AND DISCUSSIONS

5.1 SIMULATION RESULTS

The proposed 3L-TI fed PMSM drive with hybrid technique is simulated in the MATLAB Simulink environment under various EV scenarios, and it is compared with the PI-controller-based vector control technique and the Conventional-MPCC technique (C-MPCC). Table 2. Presents the details of the PMSM used in the experiment. In this complete article, the sequence followed for the convenience of comparison is the first technique is PI controller-based vector control, the second is C-MPCC, and the third is the proposed ANFIS-FCS-MPCC technique.

To validate the proposed ANFIS-FCS-MPCC approach and compare it against traditional PI-controller-based vector control and Classical MPCC (C-MPCC), simulations were performed on a 3L-TI-fed PMSM drive under various dynamic and steady-state conditions. The PI controller was implemented using the ZN method, featuring an anti-windup mechanism to minimize the adverse effects of integral gain during rapid speed changes.

PI controller gains calculations using the ultimate gain method by ZN:

This method involves the calculation of the ultimate gain (K_u) and the ultimate period (T_u). K_u is the gain of the proportional controller (K_p) at which the output of the loop provides sustained oscillations, and the period of oscillations is T_u. This is done by running the control loop at the verge of instability with a simple proportional closed-loop controller. The value of the gain K_p at which the system becomes marginally stable is equal to the ultimate gain K_u. The empirical formula by ZN for the gains of the PI controller is given by:

$$K_p = 0.45 * K_u \tag{30}$$

$$K_i = 1.2 * \frac{K_u}{T_u} \tag{31}$$

$$K_a = \frac{1}{K_i} \tag{32}$$

(a) Current control inner loop:

$$G(s) = \frac{1}{\tau_i s + 1} \tag{33}$$

$$\tau_i = \frac{L_q}{R_s} = \frac{3.285mH}{1.535\Omega} \approx 2.14ms \tag{34}$$

By Ziegler and Nichols' estimation method, the value of the ultimate gain K_u and T_u is calculated by:

$$K_u = \frac{1}{K} = \frac{1}{1/R_s} \approx 1.5 \tag{35}$$

$$T_u \approx 2 * \tau_i \approx 4.28ms \tag{36}$$

Now, putting the values of K_u and T_u in the equation. 27, 28, and 29, the current control loop PI controller gains can be calculated as:

$K_{pd} = K_{pq} = 0.675$, $K_{id} = K_{iq} = 420$, and $K_{ad} = K_{aq} = 0.00238$.

(b) Speed control outer loop:

$$K_t = 1.5 * p * \lambda_{PM} = 0.594 Nm / A \quad (37)$$

The values of K_u and T_u are 0.8 and 15ms respectively, therefore putting these values in equation. 27, 28 and 29, the speed control loop PI controller gains are calculated as $K_{p\omega} = 0.36$, $K_{i\omega} = 64$, and $K_{a\omega} = 0.0156$. Table 3. Includes the PI controller gains.

All the controllers are manually tuned for zero offset error in speeds. For a fair comparison, C-MPCC and the proposed ANFIS-FCS-MPCC were also tested under identical reference conditions. The proposed method replaces the PI controllers in both the inner and outer control loops. Additionally, an optimal switching vector selection method was applied in MPCC to maintain a low average SF, while leveraging the robustness, adaptiveness, and accuracy of ANFIS combined with MPCC.

5.1.1 Analysis of dynamic responses

To analyze the system's dynamic response, a reference speed of 4600 RPM was commanded at 0.05 seconds (s), and a 2 Nm load torque was applied. The results in Figure 7, show that the speed overshoot for the PI controller, C-MPCC, and proposed ANFIS-FCS-MPCC were 70, 55, and 34 RPM, respectively. The corresponding speed errors were +25, +11, and +4 RPM, while torque ripples were recorded as ±1 Nm, ±0.55 Nm, and ±0.2 Nm. The proposed method also significantly improved the stator current quality, as the reference iq current provided by the ANFIS controller exhibited almost no fluctuations, which helped the MPCC control the PMSM's stator current more effectively.

Figure 8 presents the stator current, speed, and torque response when a sudden load change occurs. At 0.6 seconds, the load drops from 2 Nm to 0, and at 0.8 s, the 2 Nm load is re-applied. The PI controller, C-MPCC, and the proposed ANFIS-FCS-MPCC technique exhibit overshoots of 75, 41, and 25 RPM, and undershoots of 125, 47, and 25 RPM, respectively. The torque ripples recorded were +0.8 Nm for the PI controller, +0.6 Nm for C-MPCC, and +0.3 Nm for the ANFIS-FCS-MPCC, demonstrating the superior performance of the ANFIS-FCS-MPCC in minimizing speed fluctuations and torque ripples.

Figure 9 shows the response when the reverse speed is commanded from +1500 to -1500 RPM is provided to the system at 3.5 s. The proposed technique achieved better performance with the lowest speed and torque ripples in all the dynamic conditions and scenarios.

5.1.2 Analysis of steady-state response

The steady-state response of the PMSM drive is presented in Figure 10 with all three techniques at 4600 RPM speed and a load torque of 2 Nm from 6 s to 10 s. The PI controller, C-MPCC, and the proposed ANFIS-FCS-MPCC exhibit steady state speed errors of 25, 6, and 2 RPM respectively. The quadrature component of the stator current is also compared and current ripples are significantly reduced in the proposed technique.

The THD in Figure 11 as a percentage of the fundamental component of stator current in steady state at 4600 rpm and 2Nm is 16.63%, 12.33%, and 9.13% for PI, C-MPCC, and proposed techniques, respectively.

5.2 EXPERIMENTAL RESULTS

The setup shown in Figure 12 has been developed for experimental analysis. The dSPACE platform with DS-1104 controller is used. To implement the proposed as well as two conventional control algorithms to control the 3L-TI fed PMSM drive and test under steady as well as various dynamic conditions.

The components of the setup are described below:

a) **dSPACE 1104:** A real-time DSP controller (PowerPC-based) for testing and implementing control algorithms. It has an MPC8240 processor with a 250 MHz CPU clock. It offers 16-bit 8 ADCs, 8 DACs, general-purpose digital inputs/outputs, 2 incremental encoders of 24 bits, and PWM interfaces well suited for rapid control prototyping (RCP) and real-time hardware in loop (HIL).
b) **Control Desk:** dSPACE graphical user interface software for real-time monitoring, parameter tuning, and data logging of control variables run on the dSPACE system.
c) **Host PC:** A Windows computer to develop Simulink models, compile code through Real-Time Interface (RTI), and interface with the dSPACE 1104 for control and data acquisition.
d) **IGBT Modules:** Insulated Gate Bipolar Transistors for three-level T-type inverter topology, (1200V, 75A) rated, to provide efficient and high-frequency switching in motor drive applications.

e) **Gate Drivers:** High-isolation driver circuits (opto-coupler-isolated) with level-shifted PWM outputs and protection features (like inbuilt deadband of 25nsec) for IGBT switch driving.
f) **DC Supply:** Programmable DC power supply (0-30 V) feeding the inverters' gate drivers and gate pulse voltage shifters.
g) **3-ph Auto Transformer:** A variable-ratio transformer to step down or control the 3-phase AC input voltage fed to the diode bridge rectifier, useful for controlled startup or variable voltage experiments.
h) **3-ph DBR:** A three-phase full-wave diode bridge rectifier to rectify the AC to unregulated DC to feed the DC bus of the inverter, for high-voltage and high-current operation.
i) **Voltage & Current Sensor Board:** Hall-effect type Phase-locked analog sensors, with isolation and conditioning circuits, are utilized for real-time sensing and feedback of phase currents and voltages to the controller.
j) **DSO:** A digital storage oscilloscope of 20 MHz bandwidth for the capturing and analysis of the switching waveforms, PWM patterns, and transient responses of the motor in the inverter-PMSM system. It has a sampling rate of up to 10 megasamples/sec.
k) **PMSM:** A 3-ph surface-mounted PMSM (1 kW, 220 V, 4600 rpm, 2.2 Nm with sinusoidal back EMF) as a test load for the motor control strategy.
l) **Inc Encoder:** Incremental Encoder, A rotary encoder (2000 PPR) with high-resolution rotor position and speed feedback to the control system for facilitating precise control.

To verify the authenticity and efficacy of the proposed controller, an investigation under steady-state and dynamic conditions of ANFIS-FCS-MPCC is conducted and evaluated against the conventional PI-based vector control and C-MPCC. Considering the operation and accuracy of each system component, such as sensors, controller, etc., the sampling frequency of the system is kept at 10 kHz. An Infinite Impulse Response (IIR) filter is used to measure the speed feedback accurately. The results of the proposed technique, conventional PI controller, and C-MPCC method presented in this section show the strength of the proposed controller when evaluated against the other two controllers.

5.2.1 Steady-State Performance Analysis

Figure 13 (a)-(c) presents the performance of the PMSM drive under steady-state conditions and compares the three methods mentioned above. The reference speed was kept at the rated 4600 rpm and the applied load was set at 2.2 Nm rated torque. For instance, the steady-state speed error was respectively ±24, ±12, and ±4 RPM. In which the proposed ANFIS-FCS-MPCC shows a 66% reduction in steady-state speed error compared to the C-MPCC technique. Similarly, the torque ripples were recorded as ±1.8, ±0.4, and ±0.22 Nm. The improvement in the quality of the three-phase stator current can also be observed for the proposed technique.

5.2.2 Dynamic Performance Analysis

Figure 14 (a)-(c) presents the performance of the three techniques in dynamic conditions when the load torque is changed instantly. Firstly, the load is applied from no load to a full load of 2.2 Nm and then removed, which is 0 Nm. The motor runs at its rated speed of 4600 RPM for the complete interval when the load is suddenly applied and removed.

5.2.3 Performance at Variable Speed

Figure 15 (a)-(c) shows the variable speed operation of the PMSM drive controlled by the three techniques with the step change in speed from 0 to 2000 RPM and 2000 to 4600 RPM, then again reduced from 4600 to 2000 RPM and then to the stop condition. The motor tracks the reference speed in all the techniques, but the speed, current, and torque ripples are minimal with the proposed technique. Figure 16 presents the graphical comparison of the %THD of stator currents for all three techniques at 4600 rpm and 2.2 Nm.

Table 4. presents the comparison of torque ripples in all three techniques at different values of speed and torque. The comparative analysis in simulation shows that the torque ripples at rated 2.2 Nm for the three techniques is 1, 0.55, and 0.2 Nm and at no load torque were recorded as 0.8, 0.6, and 0.3 Nm respectively. The comparative experimental analysis of the three discussed techniques shows that the torque ripples at 2.2 Nm rated load were recorded as 1.8, 0.4, 0.22 Nm and at no load as 1.1, 0.5, 0.25 Nm respectively. The simulation and experimental data of torque ripples at rated and no load shows the accuracy and control efficacy of the proposed technique.

Figure 17. shows the comprehensive evaluation of the three techniques. The data in the bar graphs indicate the high-quality performance of the proposed technique when compared with the conventional PI controller and C-MPCC techniques. All the simulation and experimental findings demonstrate the efficacy of the proposed approach.

Acknowledgements:

This work is carried out in the Advanced Power Electronics and Drives Laboratory of the Department of Electrical Engineering, MANIT Bhopal, INDIA.

6. CONCLUSION

This paper proposed a new hybrid ANFIS-FCS-MPCC-based controller to control a three-level T-type inverter-fed PMSM drive for EV applications. The proposed hybrid ANFIS-FCS-MPCC-based controller has been compared with conventional PI and C-MPCC-based controllers. The proposed technique has also been tested under various steady-state and dynamic conditions for EV applications. Finally, the simulation results are validated with an experimental setup developed in the laboratory. The simulation and experimental results demonstrate the effectiveness of the proposed technique. Assessment of the dynamic performance of the laboratory PMSM drive prototype is done under variable operating circumstances, using the proposed ANFIS-FCS-MPCC in contrast to other control methodologies. The proposed technique resulted in a notable reduction, including a 66% drop in torque oscillations, a 50% reduction in speed overshoots, and a 33% minimization of current harmonic distortion, in comparison to the C-MPCC method. Therefore, it can be adopted in EVs as a highly efficient control technique due to its unique features, simplicity, and efficiency.

The future work will include the following:

a) Expand ANFIS functionality for current control, accounting for discrepancies in both electrical and mechanical parameters.
b) Implementation of the proposed technique using FPGA-based processors to execute the control system at a higher sampling frequency, and then its implementation in EV prototypes.

REFERENCES

1. Le, H., Dekka, A., Ronanki, D., "Modeling and control of a new five-level converter for medium-voltage drive systems," IEEE Transactions on Transportation Electrification, **10**(2), pp. 3782–3791 (2024). https://doi.org/10.1109/TTE.2023.3312211.

2. Yang, Y., Xiao, Y., Fan, M., et al., "A novel continuous control set model predictive control for LC-filtered three-phase four-wire three-level voltage-source inverter," IEEE Transactions on Power Electronics, **38**(4), pp. 4572–4584 (2023). https://doi.org/10.1109/TPEL.2023.3233995.

3. Le, H., Dekka, A., "Optimal voltage level-based sequential predictive current control with reduced complexity for multilevel inverters," IEEE Transactions on Power Electronics, **40**(1), pp. 1272–1288 (2025). https://doi.org/10.1109/TPEL.2024.3481452.

4. Sathik, M.J., Gopinath, N.P., Hota, A., et al., "Improved dual boost mid-point clamped five-level inverter topology," IEEE Transactions on Circuits and Systems II: Express Briefs, **71**(6), pp. 3221–3225 (2024). https://doi.org/10.1109/TCSII.2024.3356171.

5. Roy, P., Banerjee, A., "A study on performance parameters of three-level T-type inverter based PMSM drives for electric vehicle applications," Electrical Engineering, **106**(2), pp. 1121–1134 (2024). https://doi.org/10.1007/s00202-023-01779-6.

6. Dharmendra Kumar, P., Ramesh, T., Ramakrishna, P., "Performance analysis of multi-level inverter-fed position sensorless PMSM drive using modified MPTC," IETE Journal of Research, **69**(9), pp. 6537–6556 (2023). https://doi.org/10.1080/03772063.2021.1999863.

7. Xu, S., Sun Z., Yao, C., et al., "Model predictive control with constant switching frequency for three-level T-type inverter-fed PMSM drives," IEEE Transactions on Industrial Electronics, **69**(9), pp. 8839–8850 (2022). https://doi.org/10.1109/TIE.2021.3114716.

8. Hota, A., Agarwal, V., "A novel leg-integrated switched capacitor inverter topology for three-phase induction motor drives," IEEE Transactions on Industrial Electronics, **71**(5), pp. 4353–4360 (2024). https://doi.org/10.1109/TIE.2023.3281694.

9. Dharmendra Kumar, P., Ramesh, T., "Investigation of torque ripple behaviour for five-level inverter-fed modified model predictive torque control-based PMSM drive," IETE Technical Review, **40**(2), pp. 252–267 (2023). https://doi.org/10.1080/02564602.2022.2086931.

10. Rathore, V., Kumar, D., Yadav, K.B., "A packed U cells multilevel inverter fed six-phase induction drive for industrial applications," Scientia Iranica, (), (2025). https://doi.org/10.24200/SCI.2025.60149.6630.

11. Schweizer, M., Kolar, J.W., "Design and implementation of a highly efficient three-level T-type converter for low-voltage applications," IEEE Transactions on Power Electronics, **28**(2), pp. 899–907 (2013). https://doi.org/10.1109/TPEL.2012.2203151.

12. Zhang, X., Bai, H., Cheng, M., "Improved model predictive current control with series structure for PMSM drives," IEEE Transactions on Industrial Electronics, **69**(12), pp. 12437–12446 (2022). https://doi.org/10.1109/TIE.2021.3134088.

13. Lingamchetty, B., Raghuwanshi, A., Ojha, A., "Battery connected multi-level inverter fed PMSM for electric vehicle applications," 2023 IEEE Renewable Energy and Sustainable E-Mobility Conference (RESEM), pp. 1–6 (2023). https://doi.org/10.1109/RESEM57584.2023.10236083.

14. Hang, J., Xia, M., Ding, S., et al., "Research on vector control strategy of surface-mounted permanent magnet synchronous machine drive system with high-resistance connection," IEEE Transactions on Power Electronics, **35**(2), pp. 2023–2033 (2020). https://doi.org/10.1109/TPEL.2019.2918683.

15. Inoue, T., Inoue Y., Morimoto, S., et al., "Maximum torque per ampere control of a direct torque-controlled PMSM in a stator flux linkage synchronous frame," IEEE Transactions on Industry Applications, **52**(3), pp. 2360–2367 (2016). https://doi.org/10.1109/TIA.2016.2531618.

16. Nasr, A., Gu, C., Wang, X., et al., "Torque-performance improvement for direct torque-controlled PMSM drives based on duty-ratio regulation," IEEE Transactions on Power Electronics, **37**(1), pp. 749–760 (2022). https://doi.org/10.1109/TPEL.2021.3093344.

17. Rathore, V., Kumar, D., Yadav, K.B., "A 5-level T-type inverter fed six-phase induction motor drive for industrial applications," International Journal of Electronics, **111**(2), pp. 259–279 (2023). https://doi.org/10.1080/00207217.2022.2164068.

18. Zhang, X., Cao, Y., Zhang, C., "Model predictive voltage control for PMSM system with low parameter sensitivity," IEEE Transactions on Industrial Electronics, **71**(11), pp. 13601–13613 (2024). https://doi.org/10.1109/TIE.2024.3376830.

19. Al-Kaf, H.A.G., Halabi, L.M., Lee, K.B., "A generalized integrated MPC-fuzzy-neural network approach for multilevel inverter fed PMSMs," IEEE Transactions on Industrial Informatics, **20**(2), pp. 2751–2761 (2024). https://doi.org/10.1109/TII.2023.3297662.

20. Jang, J.-S.R., "ANFIS: adaptive-network-based fuzzy inference system," IEEE Transactions on Systems, Man, and Cybernetics, **23**(3), pp. 665–685 (1993). https://doi.org/10.1109/21.256541.

21. Samada, S.E., Puig, V., Nejjari, F., "Robust TS-ANFIS MPC of an autonomous racing electrical vehicle considering the battery state of charge," IEEE/ASME Transactions on Mechatronics, **28**(2), pp. 656–667 (2023). https://doi.org/10.1109/TMECH.2023.3235906.

22. Nguyen, T.T., Tran, H.N., Nguyen, T.H., et al., "Recurrent neural network-based robust adaptive model predictive speed control for PMSM with parameter mismatch," IEEE Transactions on Industrial Electronics, **70**(6), pp. 6219–6228 (2023). https://doi.org/10.1109/TIE.2022.3198255.

23. Zhang, X., Liu, Z., Zhang, P., et al., "Model predictive current control for PMSM drives based on nonparametric prediction model," IEEE Transactions on Transportation Electrification, **10**(1), pp. 711–719 (2024). https://doi.org/10.1109/TTE.2023.3293512.

24. Zhang, X., Bai, H., Cheng, M., "Improved model predictive current control with series structure for PMSM drives," IEEE Transactions on Industrial Electronics, **69**(12), pp. 12437–12446 (2022). https://doi.org/10.1109/TIE.2021.3134088.

25. Vazquez, S., Rodriguez, J., Rivera, M., et al., "Model predictive control for power converters and drives: advances and trends," IEEE Transactions on Industrial Electronics, **64**(2), pp. 935–947 (2017). https://doi.org/10.1109/TIE.2016.2625238.

26. Harbi, I., Rodriguez, J., Liegmann, E., et al., "Model-predictive control of multilevel inverters: challenges, recent advances, and trends," IEEE Transactions on Power Electronics, **38**(9), pp. 10845–10868 (2023). https://doi.org/10.1109/TPEL.2023.3288499.

27. Jiang, X., Yang, Y., Fan, M., et al., "An improved implicit model predictive current control with continuous control set for PMSM drives," IEEE Transactions on Transportation Electrification, **8**(2), pp. 2444–2455 (2022). https://doi.org/10.1109/TTE.2022.3144667.

28. Xu, S., Sun, Z., Yao, C., et al., "Model predictive control with constant switching frequency for three-level t-type inverter-fed PMSM drives," IEEE Transactions on Industrial Electronics, **69**(9), pp. 8839–8850 (2022). https://doi.org/10.1109/TIE.2021.3114716.

29. Gao, J., Gong, C., Li, W., et al., "Novel compensation strategy for calculation delay of finite control set model predictive current control in PMSM," IEEE Transactions on Industrial Electronics, **67**(7), pp. 5816–5819 (2020). https://doi.org/10.1109/TIE.2019.2934060.

30. Sirsa, A., Mittal, A., Ojha, A., "A novel reconfigurable reduced switch multilevel inverter for renewable applications," Electrical Engineering, **107**, pp. 6021–6035 (2025). https://doi.org/10.1007/s00202-024-02866-y.

31. Raghuwanshi, A., Ojha, A., "An overview of the regenerative braking technique and energy storage systems in electric, hybrid, and plug-in hybrid electric vehicles," 2023 IEEE International Students' Conference on Electrical, Electronics and Computer Science (SCEECS), pp. 1–6 (2023). https://doi.org/10.1109/SCEECS57921.2023.10063062.

32. Gawhade, P., Ojha, A., "A novel design of basic module-based multilevel inverter for symmetrical/asymmetrical sources," International Journal of Circuit Theory and Applications, **51**(9), pp. 4257–4275 (2023). https://doi.org/10.1002/cta.3638.

Figures and captions:

Figure 1. 3L-TI -driven PMSM drive
Figure 2. Orientation of Space vectors for the 27 switching states
Figure 3. Structure of ANFIS controller
Figure 4. Schematic of ANFIS model as outer speed controller
Figure 5. Block Diagram of the Proposed ANFIS-FCS-MPCC for 3L-TI-driven PMSM drive
Figure 6. Flowchart of the execution sequence of the proposed ANFIS-FCS-MPCC technique
Figure 7. Simulation results of (i) speed response at 4600 rpm, (ii) torque response at 2 Nm, and (iii) stator current with (a) PI controller (b) C-MPCC (c) Proposed ANFIS-FCS-MPCC
Figure 8. Simulation results of a step change in torque at 0.6 sec and 0.8 sec (i) speed response at 4600 rpm, (ii) torque response, and (iii) stator current with (a) PI controller (b) C-MPCC (c) Proposed ANFIS-FCS-MPCC
Figure 9. Simulation results of speed reversal (i) speed response, (ii) Zoomed view of speed response, and (iii) Torque response with (a) PI controller (b) C-MPCC (c) Proposed ANFIS-FCS-MPCC
Figure 10. Simulation results of Steady state (i) speed response at 4600 rpm, (ii) Current Iq, and (iii) stator current Ia (iv) Line Voltage Vab of 3L-TI, with (a) PI controller (b) C-MPCC (c) Proposed ANFIS-FCS-MPCC
Figure 11. %THD of Current, with (a) PI controller (b) C-MPCC (c) Proposed ANFIS-FCS-MPCC
Figure 12. Experimental Setup for the 3L-TI-fed PMSM drive
Figure 13. Experimental results of steady-state response at 4600 rpm speed and 2.2 Nm load of (a) PI controller, (b) C-MPCC, and (c) Proposed ANFIS-FCS-MPCC
Figure 14. Experimental results of dynamic response at 4600 rpm speed and a load of 2.2 Nm applied for some time (a) PI controller, (b) C-MPCC, and (c) Proposed ANFIS-MPCC
Figure 15. Experimental results of the dynamic response of PMSM at variable speeds and a load torque of 2.2 Nm wit*h* (a) PI controller, (b) C-MPCC, and (c) Proposed ANFIS-MPCC
Figure 16. Comparison of Stator current Percentage THD of three techniques

Figure 17. Comparison of three techniques, (1) PI controller, (2) C-MPCC, and (3) Proposed ANFIS-MPCC, (a) Initial Speed Overshoot, (b) % THD Stator Current, (c) Steady-state speed error, (d) Steady-state Torque ripples, (e) Speed Overshoot, (f) Speed Undershoot, (S: Simulation) and (E: Experimental)

Tables and captions:

Table 1. Switching states and phase output of 3L-TI
Table 2. PMSM Parameters
Table 3. PI controller gains
Table 4. Comparison of three techniques based on torque ripples

Figures

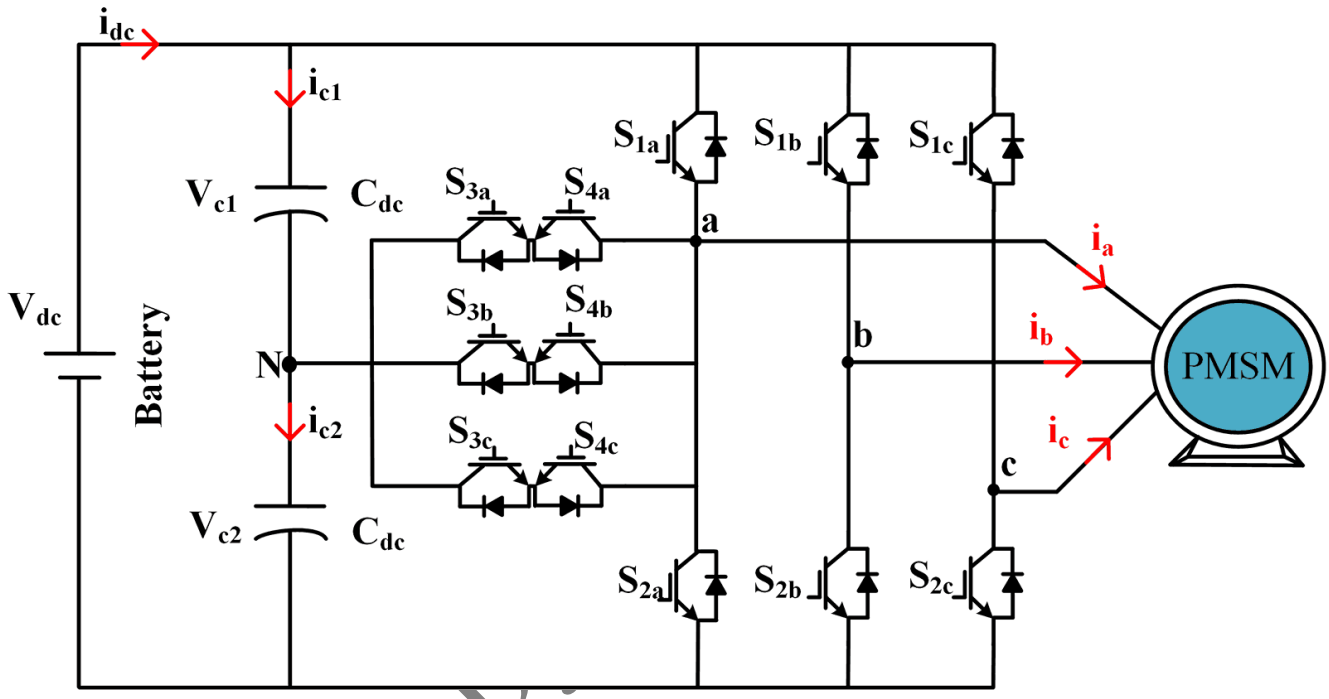

Figure 1. 3L-TI -driven PMSM drive

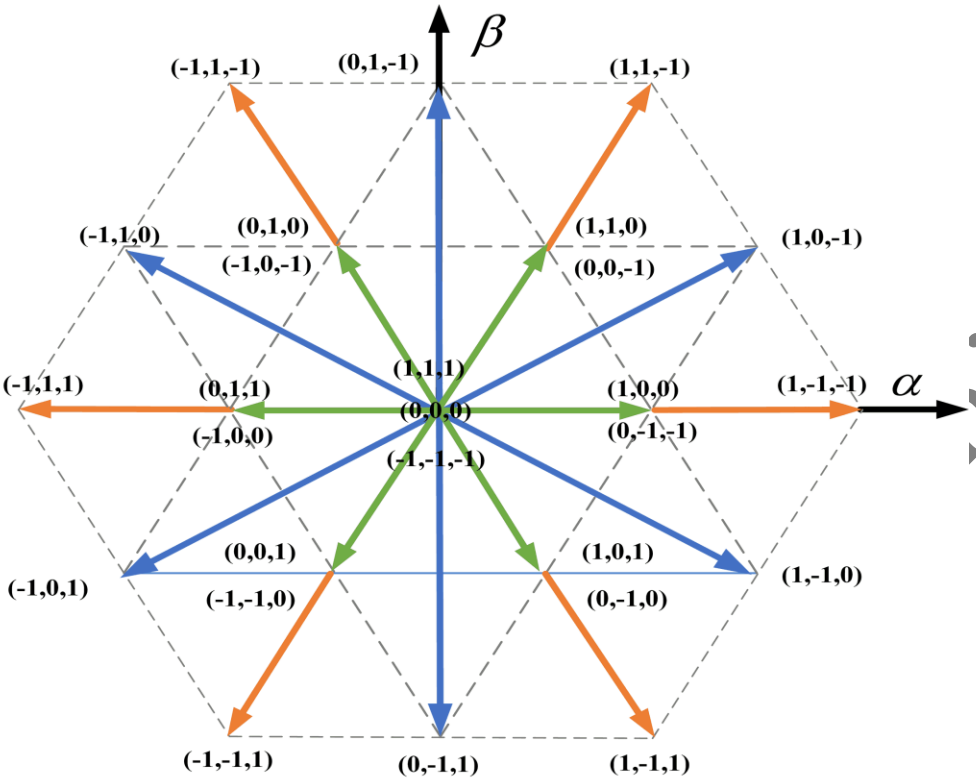

Figure 2. Orientation of Space vectors for the 27 switching states

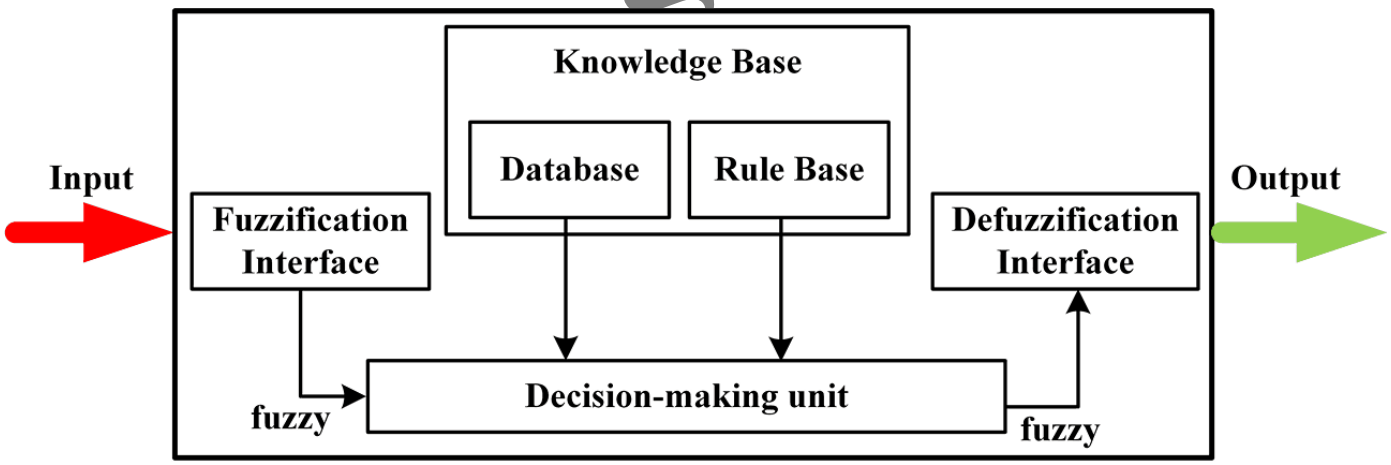

Figure 3. Structure of ANFIS controller

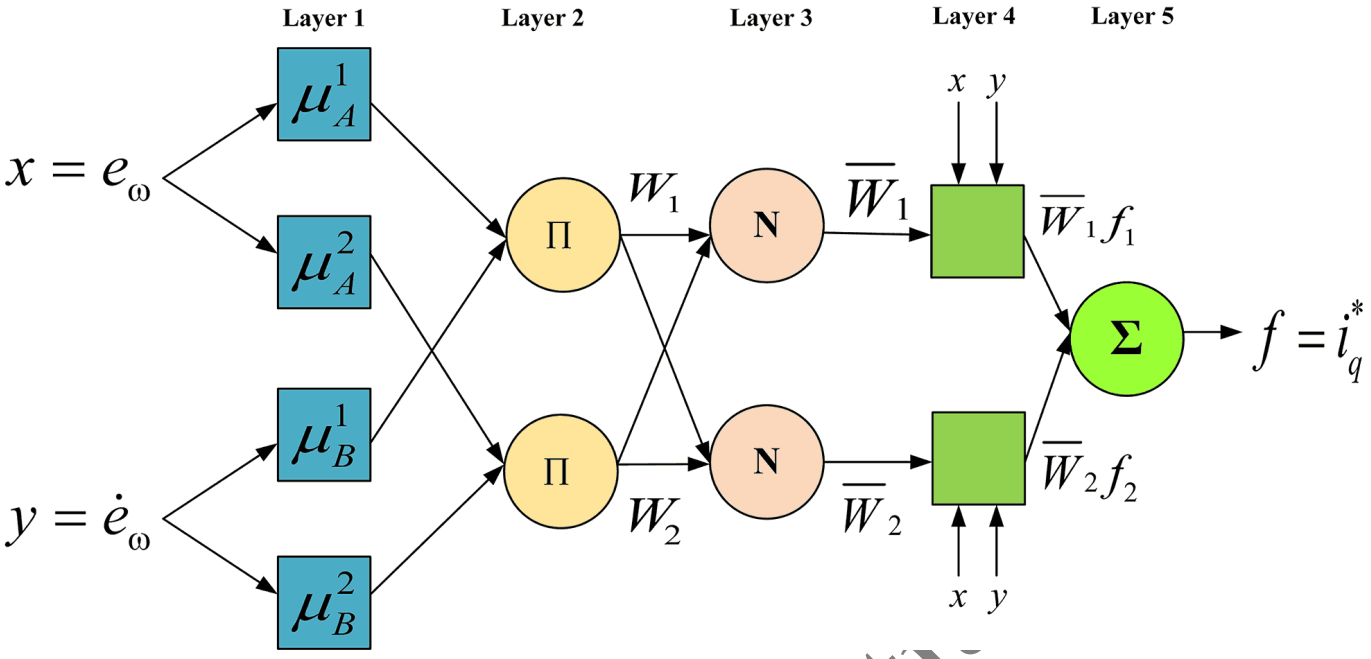

Figure 4. Schematic of ANFIS model as outer speed controller

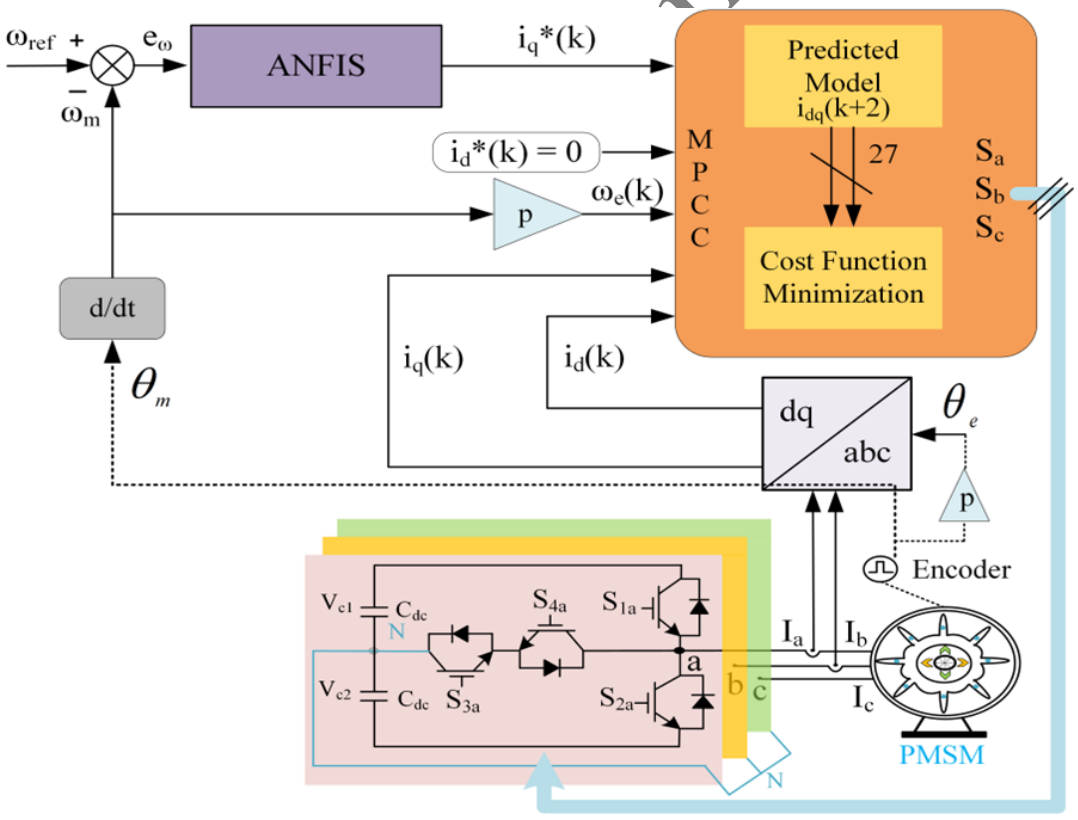

Figure 5. Block Diagram of the Proposed ANFIS-FCS-MPCC for 3L-TI-driven PMSM drive

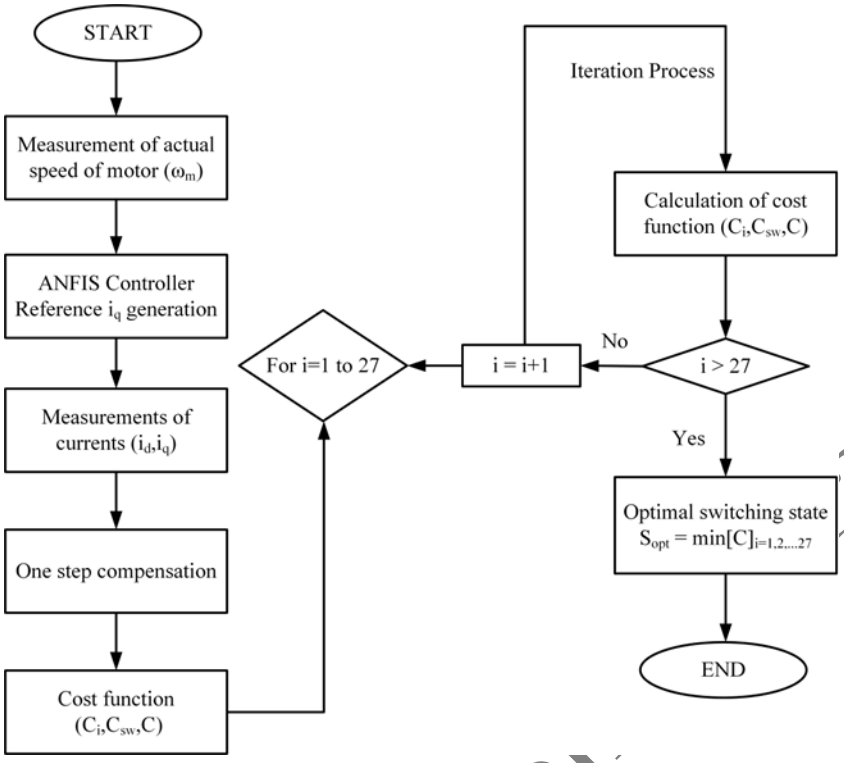

Figure 6. Flowchart of the execution sequence of the proposed ANFIS-FCS-MPCC technique

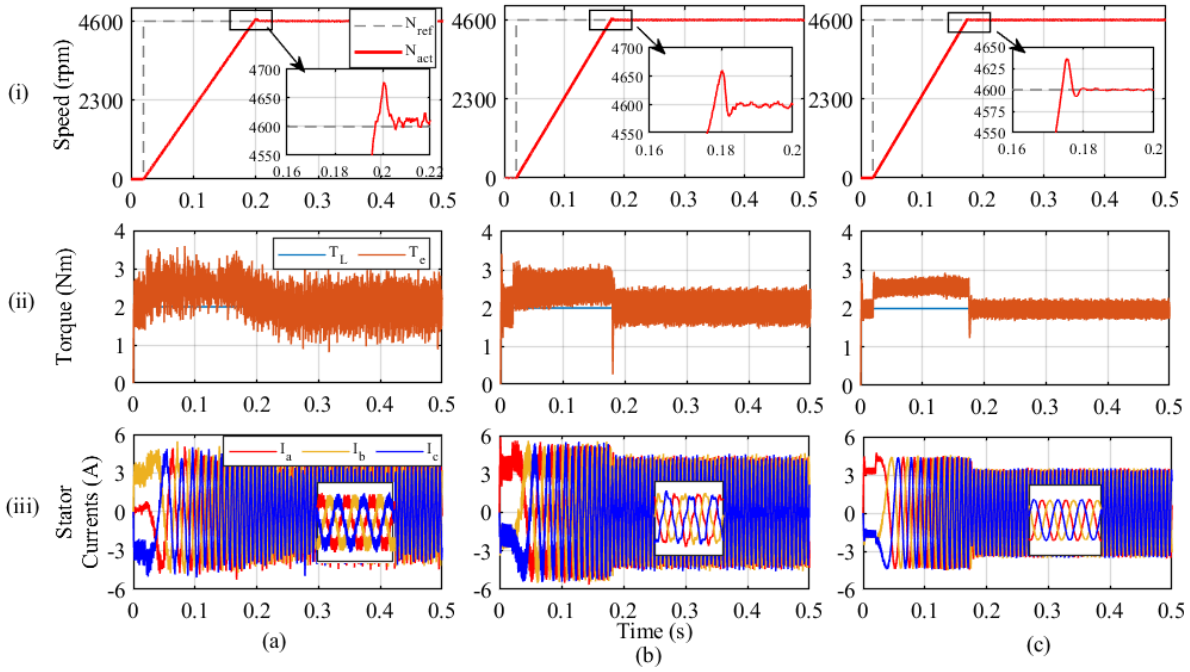

Figure 6. Simulation results of (i) speed response at 4600 rpm, (ii) torque response at 2 Nm, and (iii) stator current with (a) PI controller (b) C-MPCC (c) Proposed ANFIS-FCS-MPCC

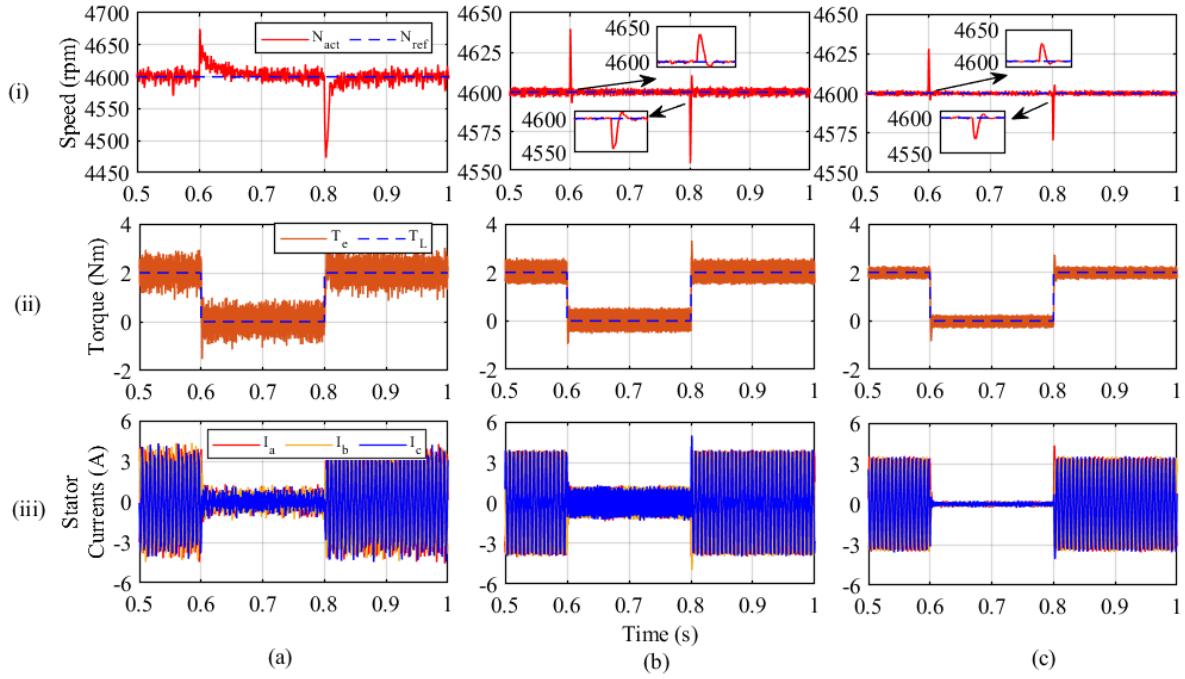

Figure 8. Simulation results of a step change in torque at 0.6 sec and 0.8 sec (i) speed response at 4600 rpm, (ii) torque response, and (iii) stator current with (a) PI controller (b) C-MPCC (c) Proposed ANFIS-FCS-MPCC

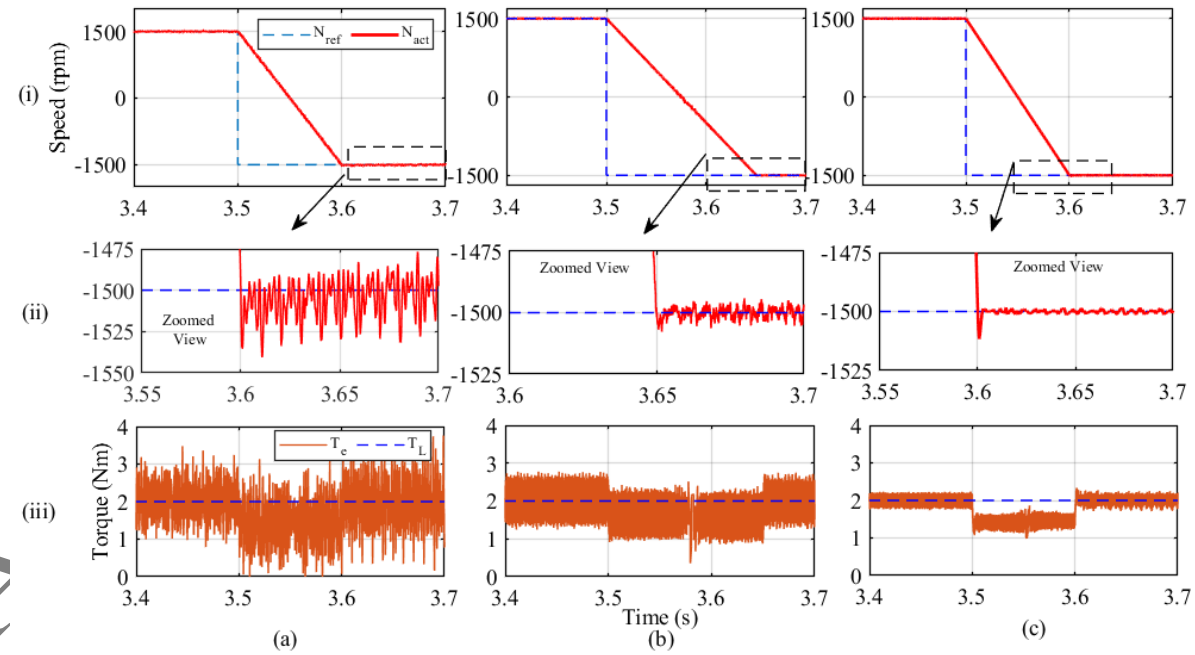

Figure 7. Simulation results of speed reversal (i) speed response, (ii) Zoomed view of speed response, and (iii) Torque response with (a) PI controller (b) C-MPCC (c) Proposed ANFIS-FCS-MPCC

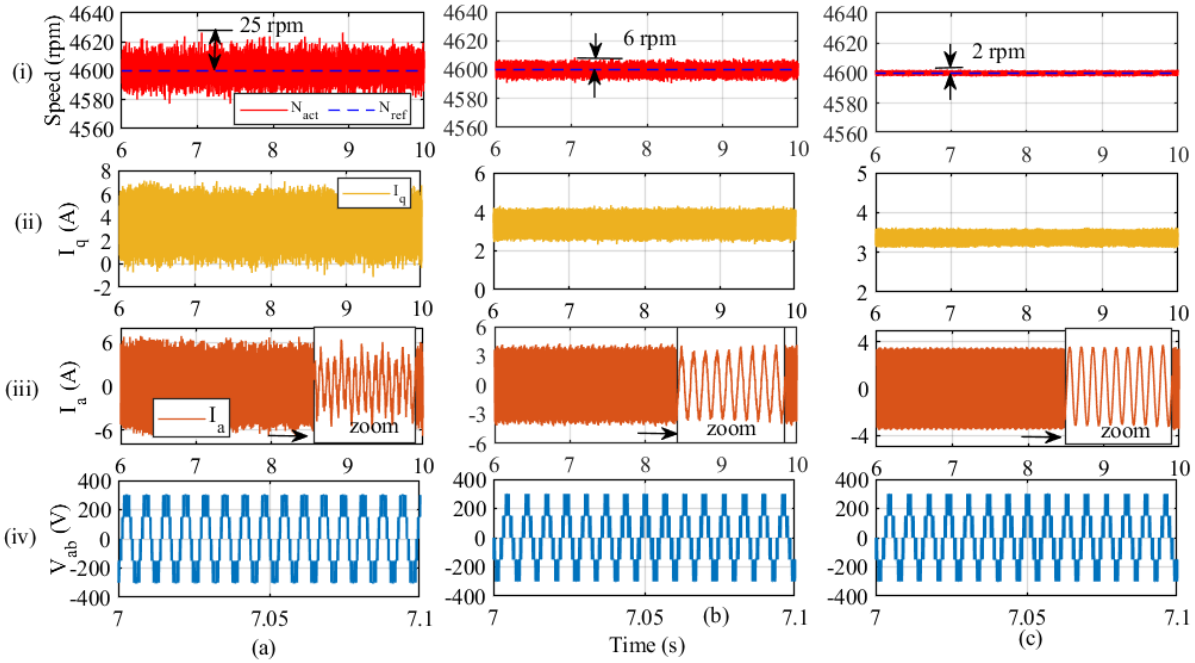

Figure 8. Simulation results of Steady state (i) speed response at 4600 rpm, (ii) Current I_q, and (iii) stator current I_a (iv) Line Voltage V_{ab} of 3L-TI, with (a) PI controller (b) C-MPCC (c) Proposed ANFIS-FCS-MPCC

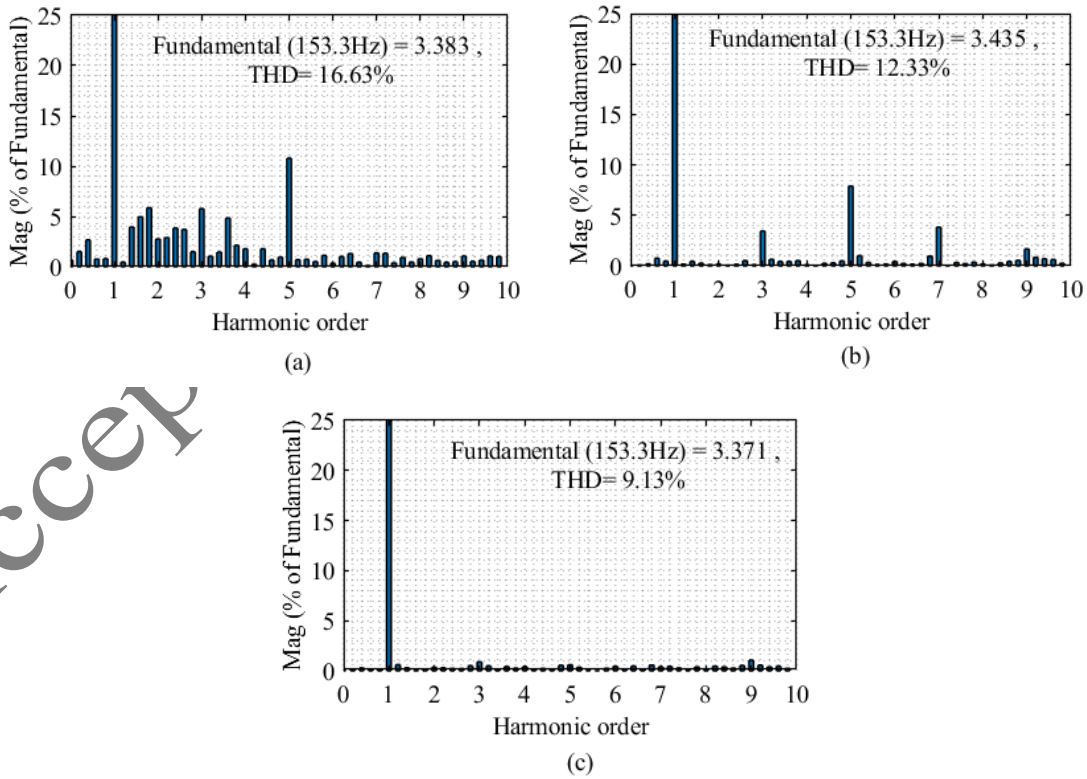

Figure 9. %THD of Current, with (a) PI controller (b) C-MPCC (c) Proposed ANFIS-FCS-MPCC

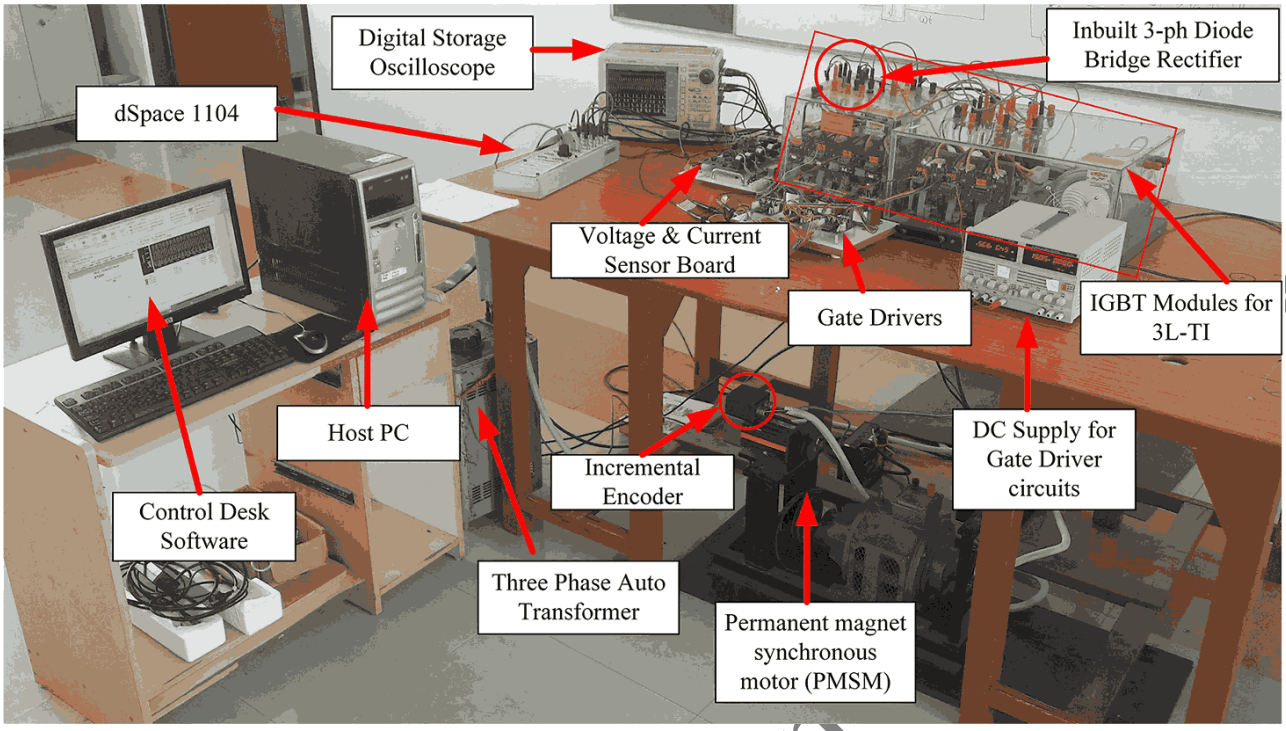

Figure 10. Experimental Setup for the 3L-TI-fed PMSM drive

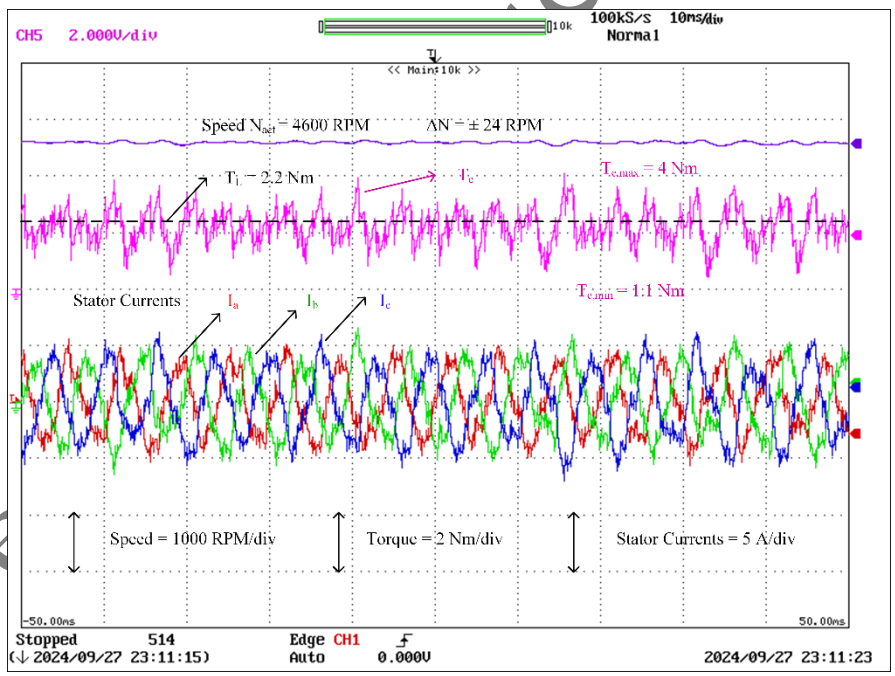

(a)

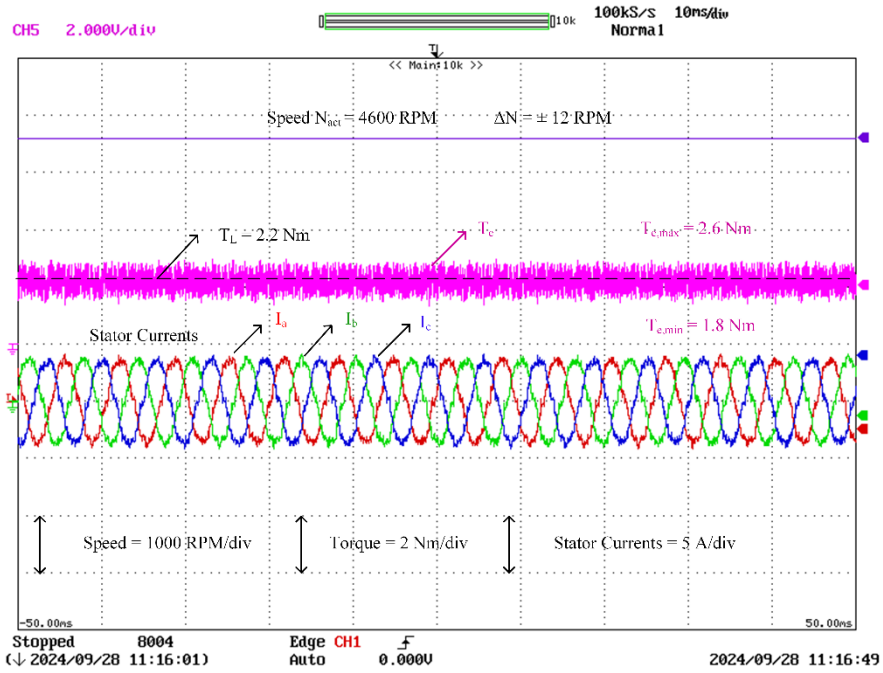

(b)

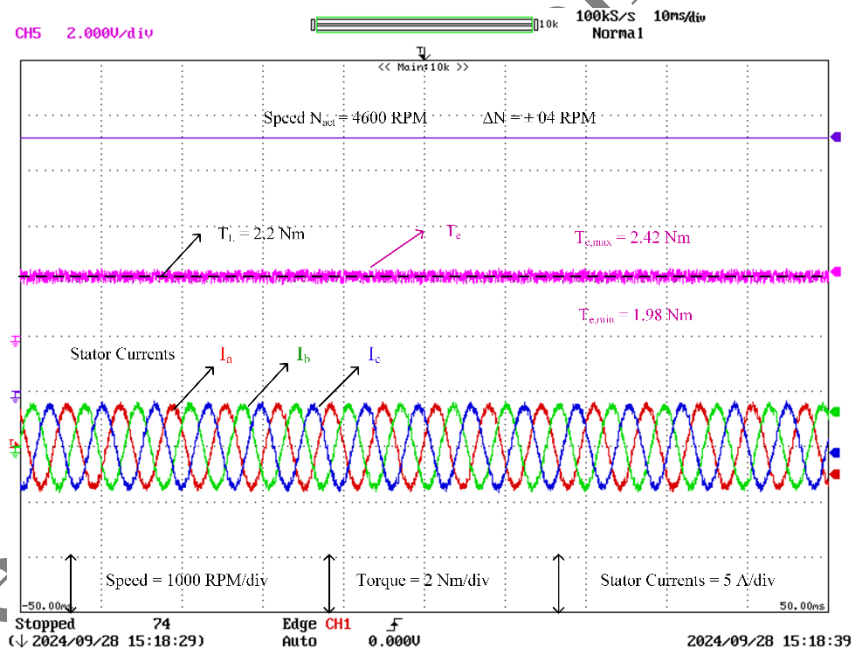

(c)

Figure 11. Experimental results of steady-state response at 4600 rpm speed and 2.2 Nm load of (a) PI controller, (b) C-MPCC, and (c) Proposed ANFIS-FCS-MPCC

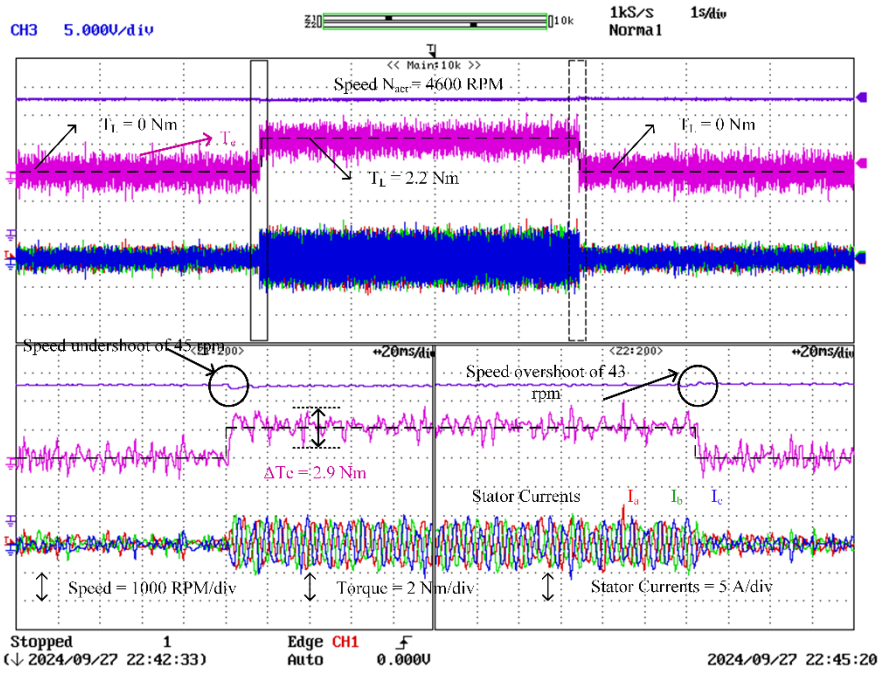

(a)

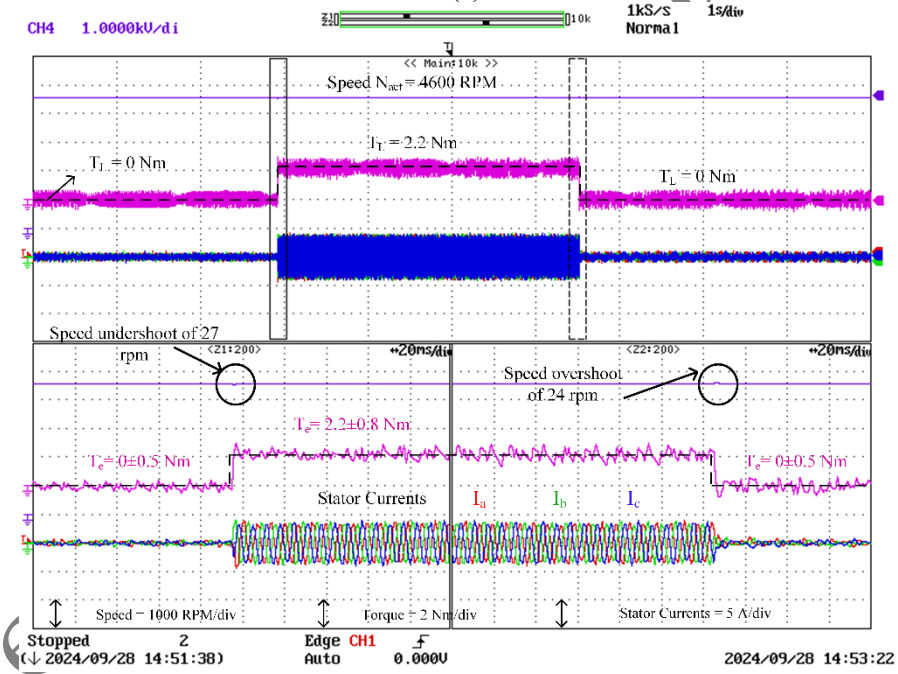

(b)

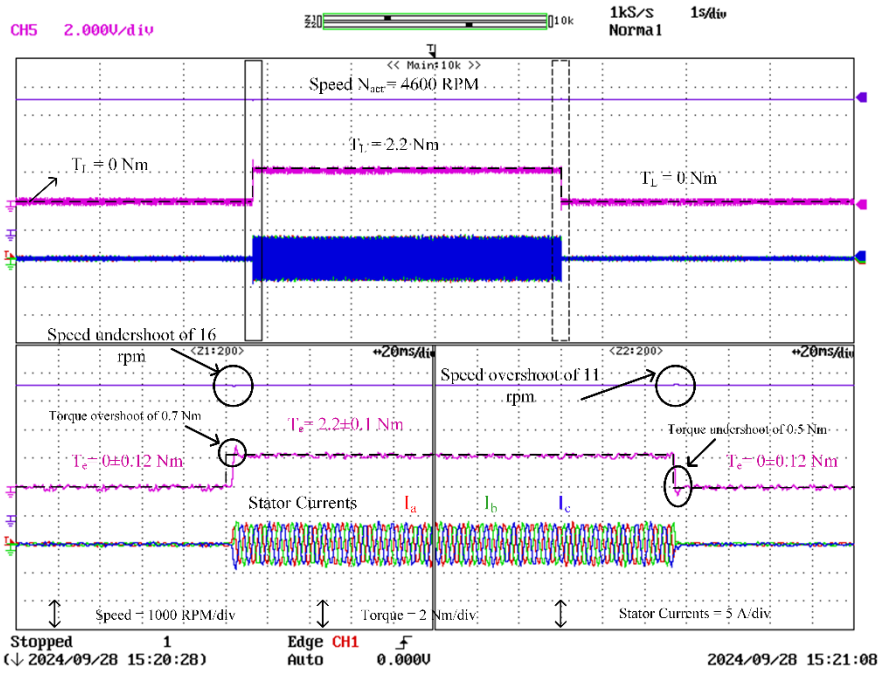

(c)

Figure 12. Experimental results of dynamic response at 4600 rpm speed and a load of 2.2 Nm applied for some time (a) PI controller, (b) C-MPCC, and (c) Proposed ANFIS-MPCC

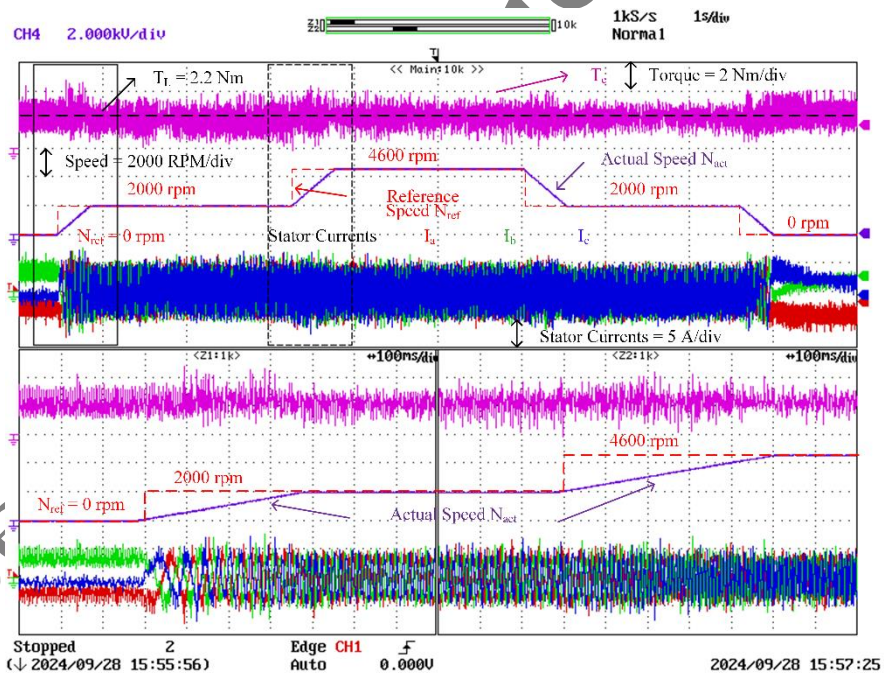

(a)

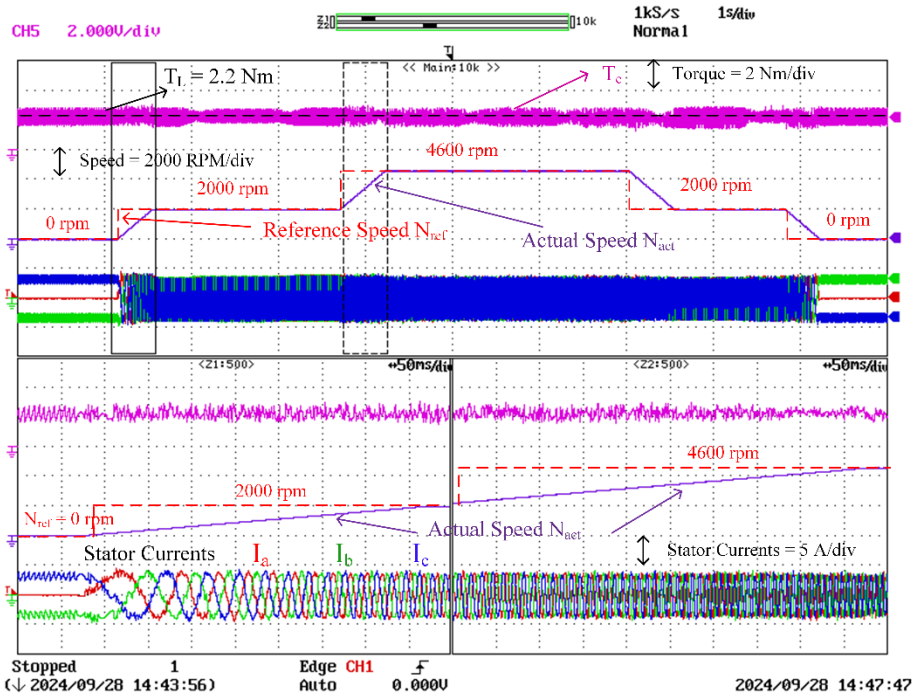

(b)

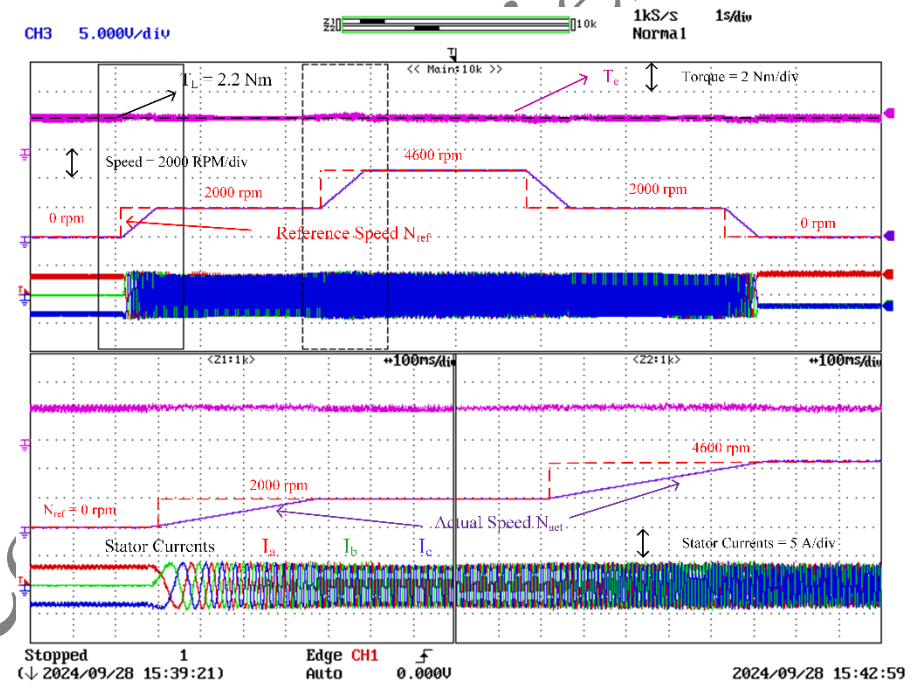

(c)

Figure 15. Experimental results of the dynamic response of PMSM at variable speeds and a load torque of 2.2 Nm with (a) PI controller, (b) C-MPCC, and (c) Proposed ANFIS-MPCC

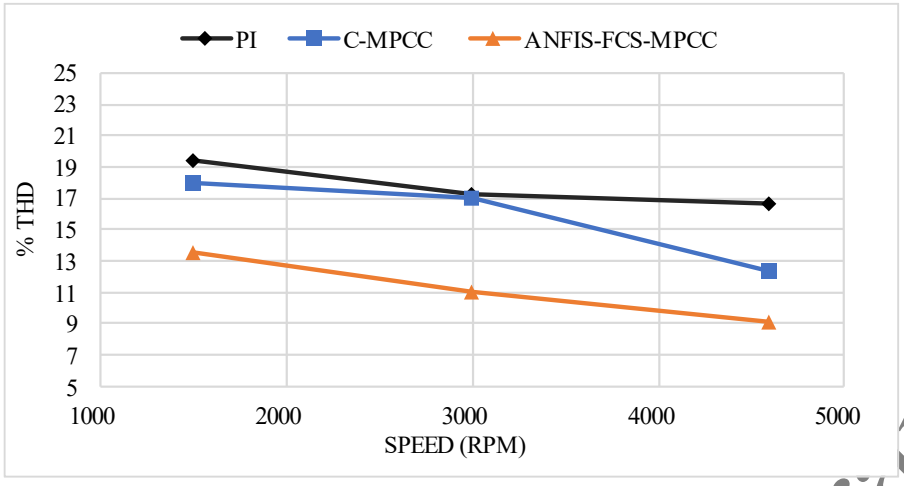

Figure 16. Comparison of Stator current Percentage THD of three techniques

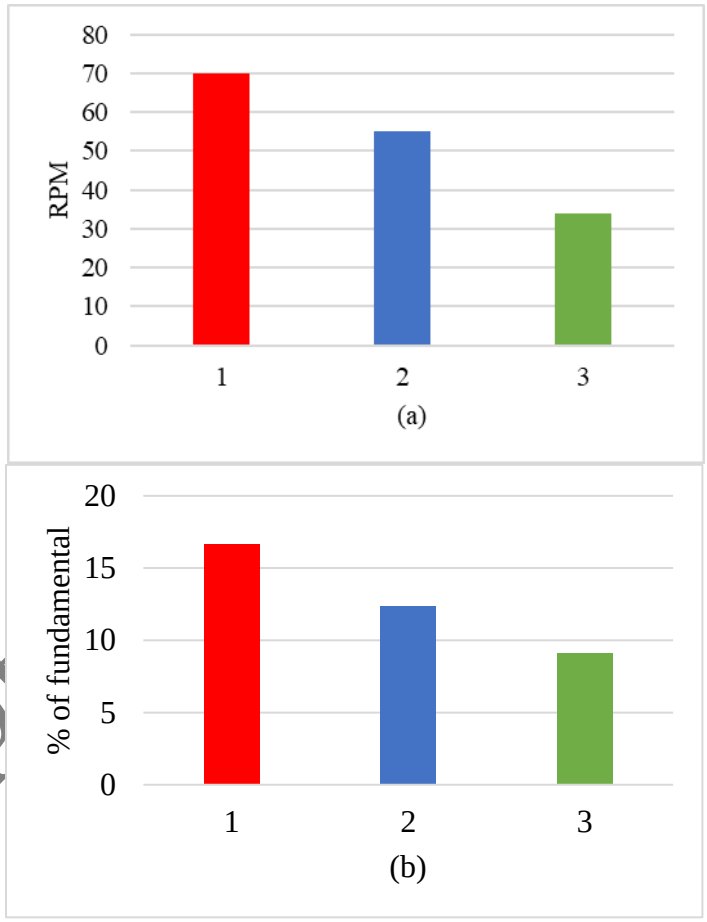

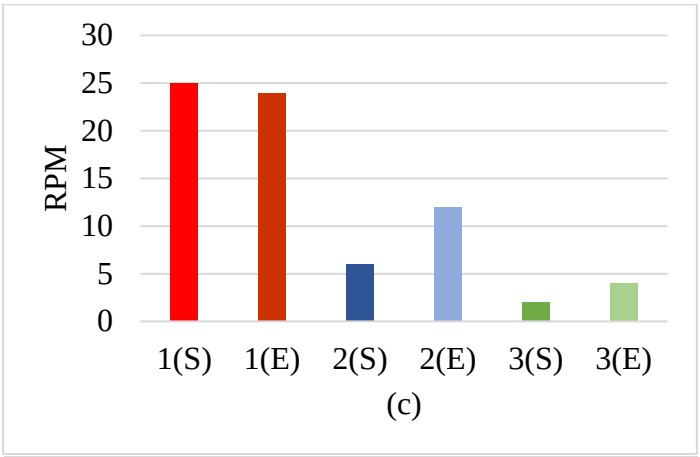

(c)

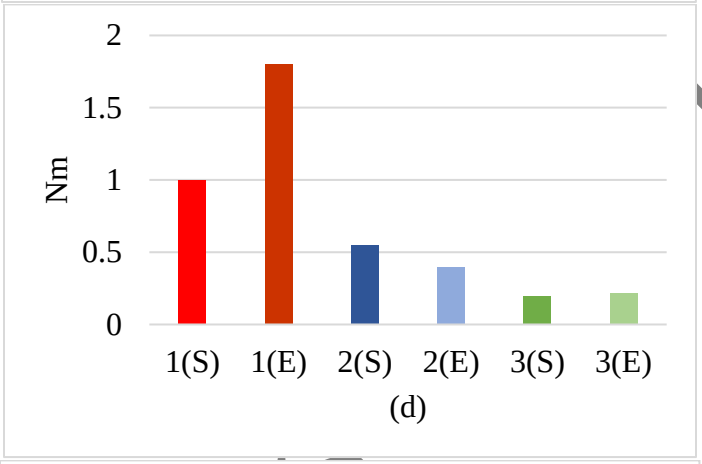

(d)

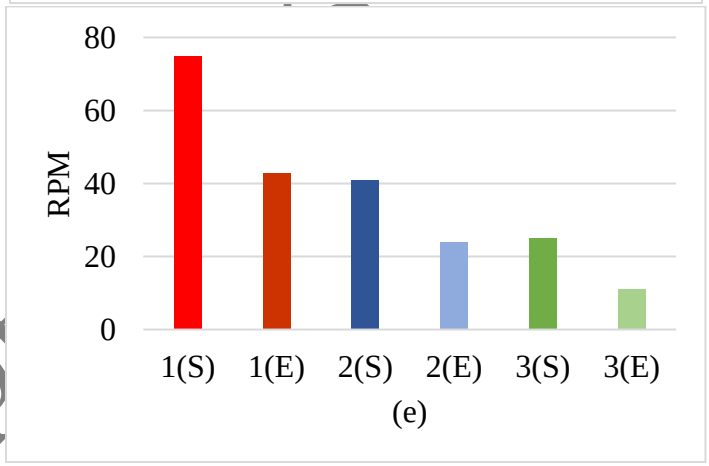

(e)

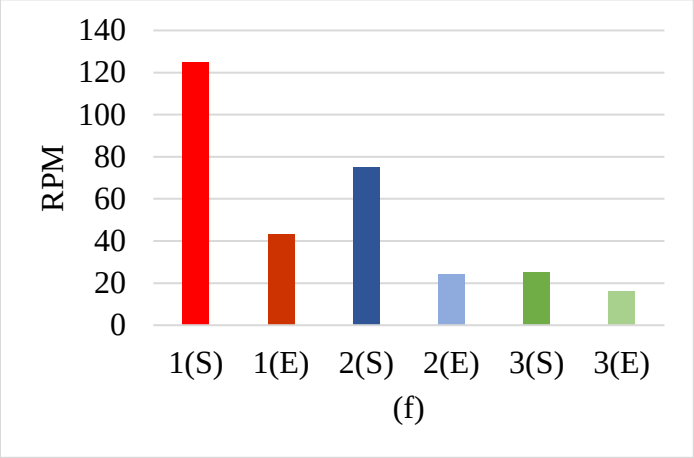

Figure 17. Comparison of three techniques, (1) PI controller, (2) C-MPCC, and (3) Proposed ANFIS-MPCC (a) Initial Speed Overshoot, (b) % THD Stator Current, (c) Steady-state speed error, (d) Steady-state Torque ripples, (e) Speed Overshoot, (f) Speed Undershoot, (S: Simulation) and (E: Experimental)

TABLES

Table 1. Switching states and phase output of 3L-TI

States	S_{1x}	S_{2x}	S_{3x}	S_{4x}	S_x	V_{xn}
[1]	1	0	1	0	1	$V_{dc}/2$
[0]	0	0	1	1	0	0
[-1]	0	1	0	1	-1	$-V_{dc}/2$

Table 2. PMSM Parameters

Parameters	Value	Parameters	Value
Power rating	1 kW	R_s	1.535 Ω
Voltage rating	220 volts	L_d	3.285 mH
Torque rating	2.2 Nm	L_q	3.285 mH
Nominal Speed	4600 rpm	DC link Voltage	300 volts
Number of Pole pairs	2	Rotor inertia	0.011 Kgm^2
DC link Capacitance	2200 µF	f_{sw}	5 kHz
Permanent magnet flux linkage	0.198 Wb	Encoder resolution	2000 ppr

Table 3. PI controller gains

Parameters	Value
Current PI	$K_{pd} = K_{pq} = 0.675$, $K_{id} = K_{iq} = 420$, $K_{ad} = K_{aq} = 0.00238$
Speed PI	$K_{p\omega} = 0.36$, $K_{i\omega} = 64$, $K_{a\omega} = 0.0156$

Table 4. Comparison of three techniques based on torque ripples

Control Technique	PI (Simulation)	C-MPCC (Simulation)	ANFIS-FCS-MPCC (Simulation)	PI (Experimental)	C-MPCC (Experimental)	ANFIS-FCS-MPCC (Experimental)
4600rpm,2.2Nm	1	0.55	0.2	1.8	0.4	0.22
4600rpm,0Nm	0.8	0.6	0.3	1.1	0.5	0.25

Biographies:

First Author- Anchal Raghuwanshi received his B.E. degree in Electrical and Electronics Engineering from Laxmi Narayan College of Technology (LNCT), Bhopal, India, in 2017, M.Tech. in Power Electronics form LNCT Bhopal, India in 2019. Currently, he is working towards pursuing his PhD at Department of Electrical Engineering, MANIT Bhopal, MP, India. His fields of interest include Multilevel inverters-based drives, Application of power converters and traction motors in electric vehicles, Hardware systems for power electronics-based drives systems, and usage of power electronics in electric vehicles.

Second Author- Amit Ojha is currently working as an Associate Professor in the Department of Electrical Engineering, MANIT Bhopal. He has completed his PhD Research Work in field of power conversion i.e. multilevel converter-based application from MANIT Bhopal. He has done his B. Tech in Electrical Engineering and M. Tech in electrical drives from MANIT Bhopal. After the completion of his PhD, he is continuously involved in the research activities. Currently Four PhD scholars are doing research under him. He has his specialization in Machines, Drives, Power Electronics, Multilevel converters. He has also authored many research articles published in SCI/SCIE/Scopus indexed journals. He has conducted various short training programs related to proposed area.